Contents

1 Introduction

The Standard Model (SM) encodes the properties of the fundamental constituents of the universe while providing a description of their interactions with one another and it describes successfully the results of a myriad of experiments, some of them to a very high level of precision.

The fundamental particles occur in two basic types called quarks and leptons, and each of the two group consists of six particles, which are related in pairs that form the three generations of matter. The lightest and most stable particles make up the first generation, whereas the heavier and less stable ones belong to the other two generations: all stable matter is made from the particles of the first generation and any heavier particle decays to lighter and more stable ones.
Three of the fundamental forces of nature result from the exchange of force-carrier particles, and the model that explains the interactions they lead to encapsulates both the theory proposed by Glashow, Salam and Weinberg, that is based on the symmetry gauge group $SU(2)_L \times U(1)_Y$ of weak left-handed isospin and hypercharge which explains and unifies the electromagnetic and weak interactions between quarks and leptons , and the strong interaction between colored quarks which was made clear by the theory of Quantum Chromo-Dynamics (QCD), based on the group $SU(3)_C$.

Problems with the Standard Model arose when it was considered that, experimentally, the weak-force bosons $W^{\pm}$ and Z appeared to be massive, breaking the proposed $SU(2)_L \times U(1)_Y$ symmetry. A mechanism to generate masses while retaining the overall gauge symmetry of the theory was proposed in 1964 by Higgs, Brout, Enlgert, Guralnik, Hagen and Kibble, following earlier theoretical work that introduced symmetry-breaking into condensed matter in the phenomenon of superconductivity as described by the theory of Bardeen, Cooper and Schrieffer, and the work by Nambu which introduced symmetry breaking to particle physics in 1960 concerning pions' masses and their low-energy couplings to protons, neutrons and each other.
The mechanism works as follows: one introduces an $SU(2)$ doublet of complex scalar fields of which the neutral component acquires a non zero vacuum- expectation-value. A consequence of this is that the once electroweak $SU(2)_L \times U(1)_Y$ symmetry is spontaneously broken to the electromagnetic $U(1)_Q$ symmetry. Three of the four degrees of freedom of the $SU(2)$ doublet are absorbed by the weak $W^{\pm}$ and Z bosons to form their longitudinal polarizations and to acquire masses, and the remaining degree of freedom corresponds to a scalar particle, the Higgs boson.
It was later showed by Weinberg that the fermion masses (which also brought problems to the overall SM theory) were in turn generated through a Yukawa interaction with the same scalar field and its conjugate field.

Building on the work done at LEP and Tevatron, on 4 July 2012, the ATLAS and CMS experiments at CERN's Large Hadron Collider (LHC) announced they had each observed a new particle in the mass region around 126 GeV.

Further measurements have shown that it appears to be consistent with the Higgs boson but it will take further work to determine whether or not it is the predicted SM Higgs particle. Other types of Higgs bosons are predicted by new theories, such as supersymmetry, that go beyond the Standard Model. The work done at LHC following the discovery also proved that the fermions' interaction strengths were consistent with their masses as predicted.

The task of determining whether the new $\sim 125\ GeV$ particle is in fact the one predicted by the Standard Model is one of the most important problems that science has to offer, and in this work we propose a way of studying the Higgs properties through its interaction with the top quark, which has the largest mass out of all the known fermions, thus rendering its coupling strength very important.
The method of calculating cross section for particles' interactions was made clear by the work of Richard Feynman, who introduced his famous "Feynman Diagrams" in a meeting in 1948 to address the problems in the quantum theory of electromagnetic interactions, QED. The diagrams were a useful compactification of all the underlying algebra and they offered a systematic way of computing the so called "S-matrix" elements, which is basically the goal of particle physics. The rules for the diagrams are obtained in roughly the following way: one inserts the QED hamiltonian in the "S-operator", which is Taylor expanded, and calculates (albeit with a lot of effort) all the infinite terms appearing in the expansion, of which each one represents a physical interaction between particles (with exceptions); it is found that every term present has powers of the same scaling constant in front (which is treated as a small parameter in the expansion), thus making it possible to neglect higher order terms: essentially a term with a power of n represents a physical process that involves n interactions, whereas higher order terms are considered corrections to this process. This process as a whole was found to be very patterned by Feynman, to the point of devising rules for it.
Despite being an incredibly useful tool for the calculation of the said cross sections, the physics community soon realized that the algebra involved in these diagrams was far too time-consuming and complex to carry out by hand, therefore the use of numerical calculations soon took over and programs like MadGraph5_aMC@NLO (used in this thesis) that integrated Feynman's rules were made available.

The top quark, being the heaviest known fermion, has the largest interaction-with-Higgs cross section, making it very useful at the LHC for the investigation of the Higgs' properties.
In this work we parametrize in the most general way (making no prior SM assumptions) the top-Higgs coupling and consider various processes in which this interaction occurs. The goal is to study the dependence of a certain channel's cross section on the parameters and then, utilizing LHC measurements, put bounds on them; combining a multitude of processes results therefore in stringent bounds on the interaction. We also make predictions for the possible rigidity of the bounds in future LHC runs with higher luminosities.

This thesis is organized as follows. In Chapter 2 we give an overview of the Standard Model, the necessity of the Higgs mechanism for generating masses and the consequent prediction for the existence of a new boson, the mass of which was left to be probed experimentally; finally we give a brief summary of the accelerators and their participation in the final discovery of the particle.
In Chapter 3 we offer an "historical" account of Feynman diagrams, their formal definition and various properties and then we touch on numerical phase space integration for the calculation of inclusive cross sections.
In Chapter 4 the results of the calculations are showed and bounds on the used parameters are graphically given and finally in Chapter 5 we also comment on further directions of our work.

2 The Higgs mechanism

2.1 The Standard Model

It is known that the Standard Model is a gauge quantum field theory (QFT) based on the following symmetry group:

$$SU(3)_C \times SU(2)_L \times U(1)_Y \tag{1}$$

since the electroweak theory, devised by Glashow-Weinberg-Salam, was shown to be a Yang-Mills theory based on the group $SU(2)_L \times U(1)_Y$ and the QCD gauge theory is modeled with the symmetry group $SU(3)_C$.
The SM presents matter fields divided in three generations of Dirac fermions which come in left-handed (l.h.) and right-handed (r.h.) chiral quarks and leptons: $f_{L,R} = \frac{1}{2}(1 \mp \gamma_5)f$. The l.h. fermions are grouped in weak isodoublets whereas the r.h. ones are to be found in weak isosinglets. Therefore for every generation we have 15 matter fields: 2 l.h. leptons and a r.h. one, 2×3 l.h. quarks and 2×3 r.h. quarks. For the purposes of the present thesis, the SM is well summarized by the following:

	Fermion Multiplets			I	I_3	Q	Y_W
Leptons	$L_1 = \begin{pmatrix}\nu_e \\ e\end{pmatrix}_L$	$L_2 = \begin{pmatrix}\nu_\mu \\ \mu\end{pmatrix}_L$	$L_3 = \begin{pmatrix}\nu_\tau \\ \tau\end{pmatrix}_L$	$1/2$	$\begin{pmatrix}+1/2 \\ -1/2\end{pmatrix}$	$\begin{pmatrix}0 \\ -1\end{pmatrix}$	$\begin{pmatrix}-1 \\ -1\end{pmatrix}$
	e_R	μ_R	τ_R	0	0	-1	-2
Quarks	$Q_1 = \begin{pmatrix}u \\ d\end{pmatrix}_L$	$Q_2 = \begin{pmatrix}c \\ s\end{pmatrix}_L$	$Q_3 = \begin{pmatrix}t \\ b\end{pmatrix}_L$	$1/2$	$\begin{pmatrix}+1/2 \\ -1/2\end{pmatrix}$	$\begin{pmatrix}+2/3 \\ -1/3\end{pmatrix}$	$\begin{pmatrix}+1/3 \\ +1/3\end{pmatrix}$
	u_R	c_R	t_R	0	0	$+2/3$	$+4/3$
	d_R	s_R	b_R	0	0	$-1/3$	$-2/3$

Table 1: Summary of fermion multiplets. L.h. doublets are displayed in parenthesis and are separated from r.h. singlets. Weak isospin I and its projection I_3 are also showed, with the respective hypercharge Y_W. Electric charges Q of the two states of a doublet are one unit of charge distant from each other; the difference $Q - I_3 = Y_W/2$ is the same inside every doublet ($-1/2$ for l.h. leptons, $+1/6$ for l.h. quarks).

The SM also includes gauge (spin-1) fields that correspond to the bosons, which mediate the interaction between the actual particles. The fields' strengths are given by:

$$\begin{aligned} G^a_{\mu\nu} &= \partial_\mu G^a_\nu - \partial_\nu G^a_\mu + g_s f^{abc} G^b_\mu G^c_\nu \\ W^a_{\mu\nu} &= \partial_\mu W^a_\nu - \partial_\nu W^a_\mu + g_2 \epsilon^{abc} W^b_\mu W^c_\mu \\ B_{\mu\nu} &= \partial_\mu B_\nu - \partial_\nu B_\mu \end{aligned} \tag{2}$$

where the tensor f^{abc} is for the structure constants of the $SU(3)_C$ group and ϵ^{abc} is the antisymmetric tensor. The field B_μ is the generator Y of $U(1)_Y$, the three fields

$W_\mu^{1,2,3}$ correspond to the three generators $T^a(a = 1, 2, 3)$ of $SU(2)_L$, where $T^a = \frac{1}{2}\tau^a$ with τ^a being the 2×2 Pauli matrices, and lastly the eight fields $G_\mu^{1,2,\cdots,8}$ correspond to the eight generators of $SU(3)_C$; g_s, g_1 and g_2 are the coupling constants of, respectively, $SU(3)_C$, $SU(2)_L$ and $U(1)_Y$.

Following the work in [1], the SM Lagrangian (excluding mass terms for fermions and bosons) is given by:

$$\begin{aligned}\mathcal{L}_{SM} = &-\frac{1}{4}G^a_{\mu\nu}G^{\mu\nu}_a - \frac{1}{4}W^a_{\mu\nu}W^{\mu\nu}_a - \frac{1}{4}B_{\mu\nu}B^{\mu\nu} \\ &+ \bar{L}_i iD_\mu\gamma^\mu L_i + \bar{e}_{R_i} iD_\mu\gamma^\mu e_{R_i} + \bar{Q}_i iD_\mu\gamma^\mu Q_i + \bar{u}_{R_i} iD_\mu\gamma^\mu u_{R_i} + \bar{d}_{R_i} iD_\mu\gamma^\mu d_{R_i}\end{aligned} \tag{3}$$

where the first row describes the Yang-Mills propagation of the gauge fields, and the second row their coupling to matter fields made by the covariant derivative, which, for instance in the case of quarks, is parametrised by:

$$D_\mu\psi = (\partial_\mu - ig_s T_a G^a_\mu - ig_2 T_a W^a_\mu - ig_1 \frac{Y_q}{2} B_\mu)\psi \tag{4}$$

It is easy to check that the said Lagrangian is invariant under local gauge transformation generated by (1). As specified above, the Lagrangian (3) does not contain mass terms for any of the fields, however, since experiments have confirmed that particles generally (with a few exceptions) have mass, those terms appear to be a requirement. Adding mass terms by brute force is a relatively easy task to accomplish, but one also needs to check that the overall theory maintains a gauge symmetry.

For the strong interactions, the gluons appear to be massless while the quarks are massive. For the latter (generally for all fermions in Table 1), adding an ordinary mass term $-m_q\bar{\psi}\psi$ seems to do the trick: it provides them masses while retaining the sought for $SU(3)_C$ symmetry.
Problems unfortunately do arise when trying to generate masses for the bosons: adding mass terms of the type $\frac{1}{2}M_V^2 W_\mu^\mu$ violates local $SU(2)_L \times U(1)_Y$ symmetry. Moreover, it is easy to check that the mass terms just added for the fermions violate certain symmetries, for instance, for an electron one has:

$$-m_e\bar{e}e = m_e\bar{e}(\frac{1}{2}(1-\gamma_5) + \frac{1}{2}(1+\gamma_5))e = -m_e(\bar{e}_R e_L + \bar{e}_L e_R) \tag{5}$$

which is non-invariant under transformations generated by isospin symmetries, since e_L is a member of an $SU(2)$ doublet and e_R of a singlet. Therefore, the problem of the origin of masses seems to be of a non-trivial nature, and has to be resolved through a more delicate mechanism. A symmetry breaking mechanism was indeed found by Higgs–Brout–Englert–Guralnik– Hagen–Kibble, which goes now under the name of "Higgs-mechanism".

2.2 Generation of boson and fermion masses

As stated above, one necessitates of a theory which describes a mechanism that equips both bosons and fermions with their respective experimental masses.
In particular, for bosons, one needs to generate masses for the three gauge bosons that mediate the weak interaction $W^{\pm}$ and Z, whereas the photon must remain massless and $U(1)_Y$ a symmetry of the theory. This can be done by adding an additional (invariant) part to (3) that describes a new spin-0 field:

$$\mathcal{L}_H = (D_\mu \phi)^\dagger (D^\mu \phi) - \mu^2 \phi^\dagger \phi - \lambda (\phi^\dagger \phi)^2 \tag{6}$$

where μ and λ are complex constants. For $\mu^2 > 0$ the potential is a parabola, whereas for $\mu^2 < 0$ it gives rise to the shape of a hat, as can be seen right below:

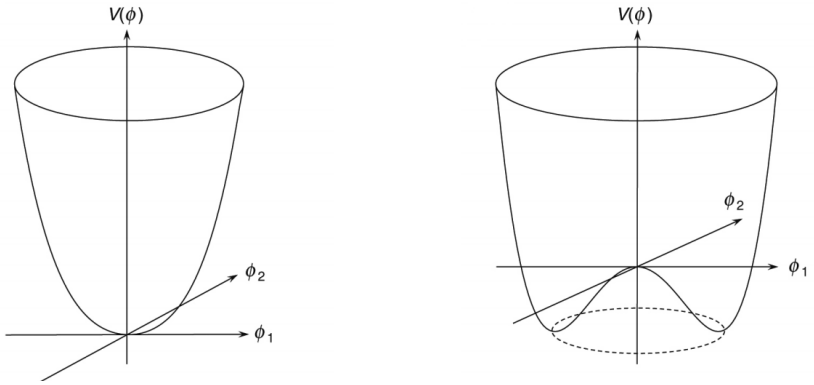

Figure 1: Shapes of the Higgs potential (6), wehere $\phi_1 = Re(\phi)$ and $\phi_2 = Im(\phi)$. On the left, for $\mu^2 > 0$, $V(\phi)$ has a parabolic form with a minimum at $V(\phi) = 0$ for $\phi_1 = \phi_2 = 0$. On the right, for $\mu^2 < 0$, the potential presents a "mexican hat" shape with minima for $V(\phi) \neq 0$.

this system is still invariant under global rotations, although not under local ones. In the case of $\mu^2 < 0$ the vacuum state $\phi = 0$ corresponds to a local maximum of the potential and thus to an unstable equilibrium point. The symmetry breaking is then completed choosing ϕ to be an $SU(2)$ doublet with defined hypercharge:

$$\phi = \begin{pmatrix} \phi^+ \\ \phi^0 \end{pmatrix} \qquad Y_\phi = 1 \tag{7}$$

Therefore the vacuum expectation value(v.e.v) of the field will be a spinor of the form:

$$\langle 0|\phi|0\rangle = \frac{1}{\sqrt{2}} \begin{pmatrix} 0 \\ v \end{pmatrix} \qquad v = \sqrt{\frac{-\mu^2}{\lambda}} \tag{8}$$

Now the potential can be expanded around the minimum, around which quantum fluctuations (that can and indeed occur) are generally parametrized by four fields $\theta_{1,2,3}(x)$ and $H(x)$:

$$\phi(x) = e^{i\theta_a(x)\tau^a(x)/v} \begin{pmatrix} 0 \\ \frac{1}{\sqrt{2}}(v + H(x)) \end{pmatrix} \tag{9}$$

then it is useful a gauge transformation:

$$\phi(x) \to \phi(x) e^{-i\theta_a(x)\tau_a(x)/v} = \begin{pmatrix} 0 \\ \frac{1}{\sqrt{2}}(v + H(x)) \end{pmatrix} \tag{10}$$

For the purpose of the generation of the boson masses, it is "only" needed to expand the term of the new Lagrangian (6) that contains the derivatives:

$$\begin{aligned} \left|D_\mu \phi\right|^2 &= \left|(\partial_\mu - i g_2 \frac{\tau_a}{2} W_\mu^a - i g_1 \frac{1}{2} B_\mu)\phi\right|^2 \\ &= \frac{1}{2}\left| \begin{pmatrix} \partial_\mu - \frac{i}{2}(g_2 W_\mu^3 + g_1 B_\mu) & -\frac{i g_2}{2}(W_\mu^1 - i W_\mu^2) \\ -\frac{i g_2}{2}(W_\mu^1 + i W_\mu^2) & \partial_\mu + \frac{i}{2}(g_2 W_\mu^3 - g_1 B_\mu) \end{pmatrix} \begin{pmatrix} 0 \\ v + H \end{pmatrix} \right|^2 \\ &= \frac{1}{2}(\partial_\mu H)^2 + \frac{1}{8} g_2^2 (v + H)^2 \left| W_\mu^1 - i W_\mu^2 \right|^2 + \frac{1}{8}(v + H)^2 \left| g_2 W_\mu^3 - g_1 B_\mu \right|^2 \end{aligned} \tag{11}$$

Now the new fields can be defined:

$$W_\mu^\pm = \frac{1}{\sqrt{2}}(W_\mu^1 \mp i W_\mu^2) \quad Z_\mu = \frac{g_2 W_\mu^3 - g_1 B_\mu}{\sqrt{g_1^2 + g_2^2}} \quad A_\mu = \frac{g_2 W_\mu^3 + g_1 B_\mu}{\sqrt{g_1^2 + g_2^2}} \tag{12}$$

so that (11) becomes:

$$\begin{aligned} \left|D_\mu \phi\right|^2 = \quad & \overbrace{\frac{1}{2}(\partial_\mu H)^2}^{\text{Higgs kinetic term}} \\ & + \overbrace{\frac{1}{4} g_2^2 v^2 W_\mu^+ W^{-\mu} + \frac{1}{8} v^2 (g_1^2 + g_2^2) Z_\mu Z^\mu}^{\text{Mass Terms}} \\ & \overbrace{\frac{1}{2} g_2^2 v H W_\mu^+ W^{-\mu} + \frac{1}{4} v H (g_1^2 + g_2^2) Z_\mu Z^\mu}^{\text{HVV coupling terms}} \\ & \overbrace{\frac{1}{4} g_2^2 H^2 W_\mu^+ W^{-\mu} + \frac{1}{8} H^2 (g_1^2 + g_2^2) Z_\mu Z^\mu}^{\text{HHVV coupling terms}} \end{aligned} \tag{13}$$

where, for clarity, HVV and HHVV are the Higgs-boson-boson and the Higgs-Higgs-boson-boson couplings.
In this way, the fact that the mass terms of the gauge fields (12) are of the following type:

$$M_W^2 W_\mu^+ W^{-\mu} \quad \frac{1}{2} M_Z^2 Z_\mu Z^\mu \quad \frac{1}{2} M_A^2 A_\mu A^\mu \tag{14}$$

leads to:

$$M_W = \frac{1}{2} v g_2 \quad M_Z = \frac{1}{2} v \sqrt{g_1^2 + g_2^2} \quad M_A = 0 \tag{15}$$

where the last equality was imposed by noticing that a term proportional to $A_\mu A^\mu$ in (13) isn't there. The original goal of generating boson masses while preserving the overall invariance of the theory is in this way accomplished: by spontaneously breaking the symmetry $SU(2)_L \times U(1)_Y \to U(1)_Q$, three Goldstone bosons have been absorbed by the $W^\pm$ and Z bosons to get their masses. Since the $U(1)_Q$ symmetry is still unbroken, its generator, which is the photon, remains massless.

As alluded to in the introduction, Weinberg showed [2] that fermion masses can in turn be generated through the same exact mechanism: using the same doublet (7) and introducing a new one $\tilde{\phi} = i\tau_2 \phi$ one completes the SM Lagrangian (3) + (6) by adding the $SU(2)_L \times U(1)_Y$ invariant Yukawa Lagrangian:

$$\mathcal{L}_F = -\lambda_e \bar{L} \phi e_R - \lambda_d \bar{Q} \phi d_R - \lambda_u \bar{Q} \tilde{\phi} u_R + h.c. \tag{16}$$

(h.c. is the hermitian conjugate). It is easy to check that the mechanism works for fermions as well by making the same assumptions from (7) to (10) and plugging them in (16); the case of the electron is quite exhaustive:

$$\begin{aligned} \mathcal{L}_F - \frac{1}{\sqrt{2}} \lambda_e (\bar{\nu}_e, \bar{e}_L) \begin{pmatrix} 0 \\ v + H \end{pmatrix} e_R + ... \\ = -\frac{1}{\sqrt{2}} (v + H) \bar{e}_L e_R \end{aligned} \tag{17}$$

where terms of the type $-m\bar{f}f$ have appeared, so that the constants that precede the fields in the second row of (17) correspond to the masses of the fermions:

$$m_e = \frac{\lambda_e v}{\sqrt{2}} \quad m_u = \frac{\lambda_u v}{\sqrt{2}} \quad m_d = \frac{\lambda_d v}{\sqrt{2}} \tag{18}$$

Now the masses of both the bosons and the fermions have been generated "at the cost" of having broken the $SU(2)_L \times U(1)_Y$ gauge symmetry. On the contrary, the electromagnetic $U(1)$ and the $SU(3)$ strong color gauge symmetries remain standing.

2.3 The Higgs particle

The last terms to be discussed in the SM Lagrangian:

$$\mathcal{L} = \mathcal{L}_{SM} + \mathcal{L}_H + \mathcal{L}_F \tag{19}$$

are the ones concerning the Higgs particle itself and its couplings to matter and gauge fields.
In (6) there remain to be expanded the terms that are not of kinetic nature, which describe the mass and the particle's self-interaction:

$$\begin{aligned} V(\phi) &= \mu^2\phi^\dagger\phi + \lambda(\phi^\dagger\phi)^2 \\ &= \frac{\mu^2}{2}(0, v+H)\begin{pmatrix}0\\v+H\end{pmatrix} + \frac{\lambda}{4}\left|(0, v+H)\begin{pmatrix}0\\v+H\end{pmatrix}\right|^2 \end{aligned} \tag{20}$$

Recalling that $v^2 = -\mu^2/\lambda$ (20) reads:

$$V = -\frac{1}{2}\lambda v^2(v+H)^2 + \frac{1}{4}\lambda(v+H)^2 \tag{21}$$

so that the part of $\mathcal{L}_H$ that concerns only the Higgs' terms becomes:

$$\begin{aligned} \mathcal{L} &= \frac{1}{2}\partial_\mu H\partial^\mu H - V(\phi) \\ &\frac{1}{2}(\partial_\mu H)^2 - \lambda v^2 H^2 - \lambda v H^3 - \frac{\lambda}{4}H^4 \end{aligned} \tag{22}$$

From this it is easy to see that the mass of the particle is:

$$M_H^2 = 2\lambda v^2 = -2\mu^2 \tag{23}$$

The Higgs boson's coupling to particles of matter and other bosons are directly found in the third and fourth rows of (13), in particular:

$$g_{Hff} = i\frac{m_f}{v} \qquad g_{HVV} = -2i\frac{M_V^2}{v} \qquad g_{HHVV} = -2i\frac{M_V^2}{v^2} \tag{24}$$

the vacuum expectation value v is completely fixed in terms of M_W or, equivalently, the weak decay Fermi constant (determined by muon decay) G_μ by (15):

$$M_W = \frac{1}{2}vg_2 = (\frac{\sqrt{2}g_2^2}{8G_\mu})^{1/2} \implies v = \frac{1}{(\sqrt{2}G_\mu)^2} \simeq 246\ GeV \tag{25}$$

whereas, since λ is not predicted by the theory, the mass of the Higgs remains to be measured experimentally.
Hadron colliders take advantage of the fact that the Higgs tends to couple preferentially to heavier particles, since the coupling constant is proportional to the mass of the particles themselves. This means that the the boson is mainly studied through its couplings with the electroweak W and Z bosons and the top and (to a lesser extent) bottom quarks, the two heaviest fermions. The four main production processes (at hadron colliders, in order of decreasing cross section) are: the gluon-gluon fusion mechanism, weak vector boson fusion processes (VBF,) associated production with W/Z bosons and with a top/bottom quark pair:

$$gg \to H \qquad \text{Gluon-gluon fusion} \tag{26a}$$
$$qq \to V^*V^* \to qq + H \qquad \text{Vector boson fusion} \tag{26b}$$
$$q\bar{q} \to V + H \qquad \text{Associated production with W/Z} \tag{26c}$$
$$gg, q\bar{q} \to Q\bar{Q} + H \qquad \text{Associated production with a heavy quark pair} \tag{26d}$$

Their Feynman diagrams are drawn below:

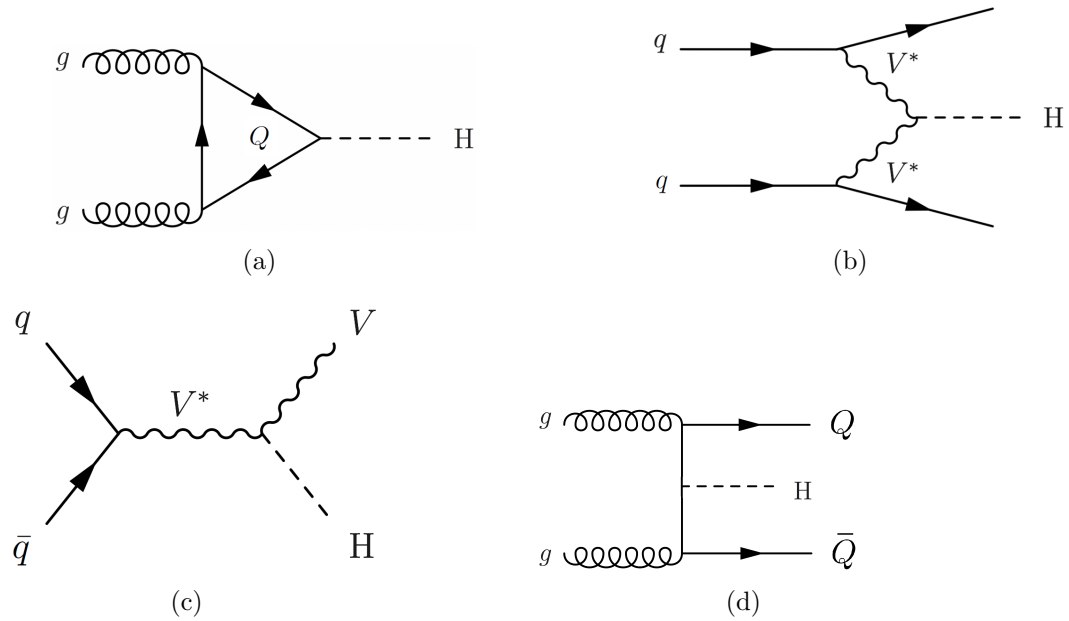

Figure 2: Feynman diagrams of the most dominant production channels of the SM Higgs boson at hadron colliders. (a)Gluon-gluon fusion , (b) Vector boson fusion, (c) Associated production with a weak vector boson and (d) Associated production with a heavy quark pair.

Naturally, there exist also additional production mechanisms for the Higgs particle, most notably it can be produced in a pair:

$$pp \to HH + X \qquad \text{Higgs pair production} \tag{27}$$

The production cross sections of the main processes above (26a)-(26d) are large

and the theoretical predictions well understood at (at least) *next-to-leading-order* NLO accuracy.

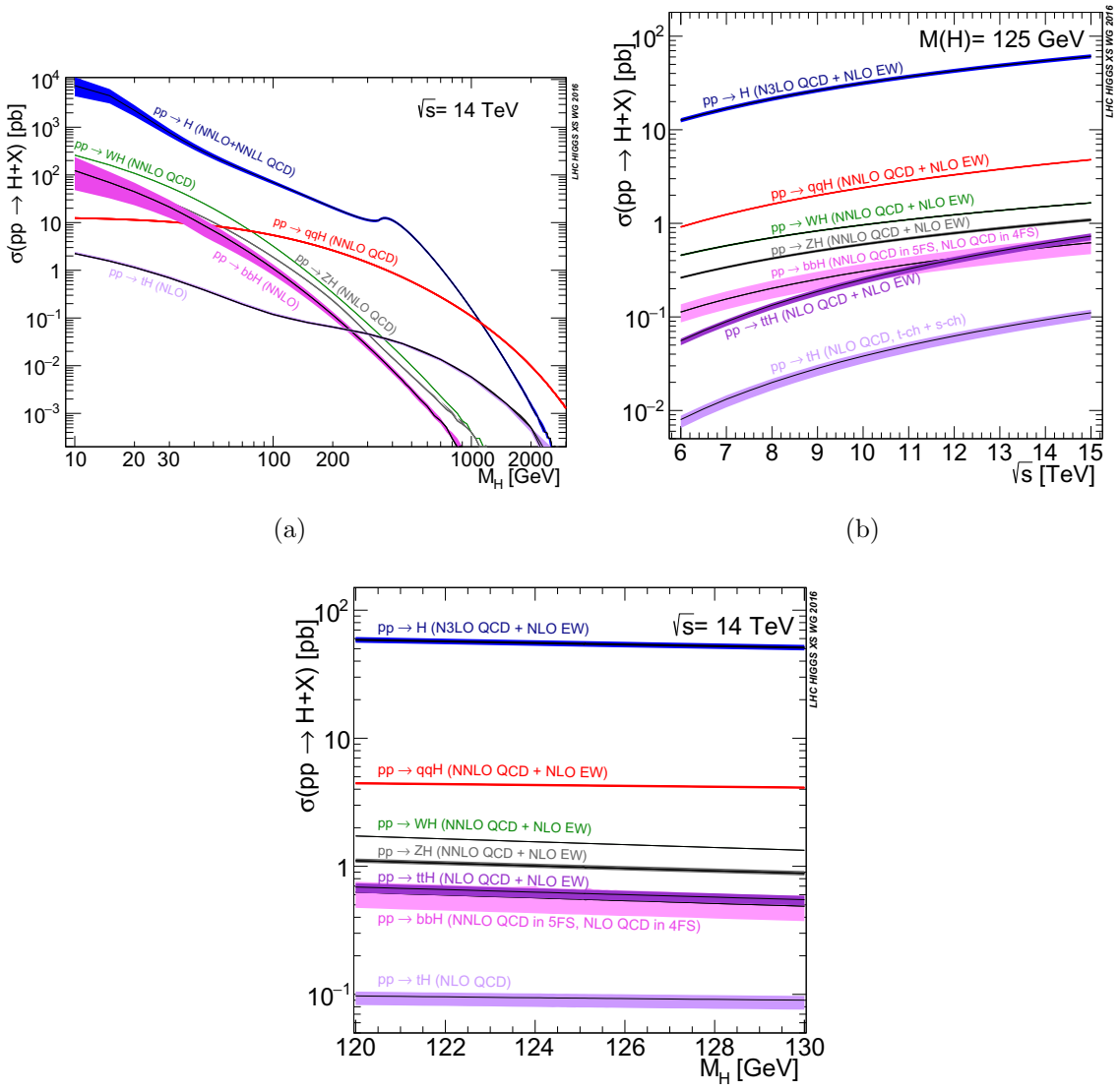

(a) (b)

(c)

Figure 3: (a) and (b) are cross sections for the production of an SM Higgs boson for the discussed processes on a mass spectrum more or less broad. (c) are the cross sections for the same processes but at a fixed Higgs mass and varying center of mass energy.

- The gluon-gluon fusion mechanism through a heavy top or bottom quark loop is the dominant production channel over a large range of the Higgs boson's mass, as can clearly be seen in Figure 3(a). Its dynamics are evidently controlled by strong interactions (mediated predominantly by the top quark loop, whereas the

bottom quark contribution remains under 10% at *leading-order* (LO)) , and as a consequence this process is known to be subject to extremely large radiative QCD corrections. At the present time and at a center of mass energy of 13 TeV (at $m_H = 125\ GeV$) we know the exact LO+NLO result for the production cross section in the SM, including all mass effects from top, bottom and charm quarks, and the NLO correction turns out to be more than 100% (for the said Higgs mass). Beyond NLO we only know the value of the cross-section in the heavy-top effective theory, and it turns out that *next-to-next-to-leading-order* (NNLO) corrections are substantial, increasing the cross section by about 30%. Recently, up to N3LO+EW (electroweak) corrections have been computed [3], which together increased the cross section by 10% more.
Our current best prediction for the total cross section of the gluon-gluon fusion mechanism is in fact N3LO+(NLO)EW, as can be seen in Figure 3(c).

- The vector boson fusion process is the second most dominant production mode for $M_H \gtrsim 100\ GeV$ whence it dominates over all the other production process, as in Figure 3(a) and (b) more clearly; in the said range, which is the most important as it is known that m_H is approximately 125 GeV, it contributes up to 50% to the total Higgs cross section. Despite its smaller cross section compared to the gluon fusion mechanism, the final state quarks take part in the formation of jets, whose signature leads to an easier job of identifying the process at accelerators. The VBF process' QCD NLO corrections at a center of mass energy of 13 TeV have been computed using the structure function approach and they increase the cross section of around 10%; also NNLO corrections have been calculated at $\sqrt{s} = 7\ TeV$ [4] (which are qualitatively the same as to the LHC's $\sqrt{s} = 14\ TeV$), and they increase the cross section by about 7% at an Higgs mass of $\approx 120\ GeV$. Finally EW corrections (known up to NLO) have been reported [5] to contribute to around 5% of the inclusive cross section in the said Higgs mass range at at $\sqrt{s} = 14\ TeV$.

- The associated production with weak W and Z bosons (also known as the "Higgs-strahlung" process) is the second most dominant production channel for $M_H \lesssim 100\ GeV$. As shown in Figure 3(c), the cross section is known up to NNLO in QCD and up to NLO for the electroweak corrections (the latter resulting in total in a 7% contribution [5]).

- The associated production with a pair of top quarks $q\bar{q}, gg \to t\bar{t}H$ plays a very important role both for the discovery of the Higgs boson and for a precise measurement of the top Yukawa coupling, because this process provides a direct way to measure it. On the other hand, the associated production of the Higgs boson with a pair of bottom quarks has a smaller cross section due to the small bottom Yukawa coupling.
QCD NLO corrections have been known for more than a decade, whereas EW corrections have only recently been calculated and turned out to be important because, for instance, they spoil the trivial dependence of the $t\bar{t}H$ cross section

on $\sim y_t^2$. EW corrections are known up to NLO and contribute in total around 4% to the inclusive cross section [5].
In some extensions of the SM, like the *Minimal Supersymmetric Standard Model* (MSSM), the coupling to the Higgs can become strongly enhanced and as a consequence this mode of production can dominate over others.

Once produced the Higgs boson decays in a fermion-antifermion pair or in gauge bosons, and since its couplings to gauge bosons and fermions are proportional to the their masses, it will tend to decay into the heaviest ones that are allowed by phase space considerations, like kinematical ones. Since the experimental masses of gauge bosons and fermions are known:

$$M_Z = 91.187\ GeV \quad M_W = 80.425\ GeV \quad m_\tau = 1.777\ GeV \quad m_\mu = 0.106\ GeV$$

$$m_t = 178 \pm 4.3\ GeV \quad m_b = 4.88 \pm 0.07\ GeV \quad m_c = 1.64 \pm 0.07\ GeV$$

the partial widths of the main Higgs boson decays can be predicted and are shown in the following figures:

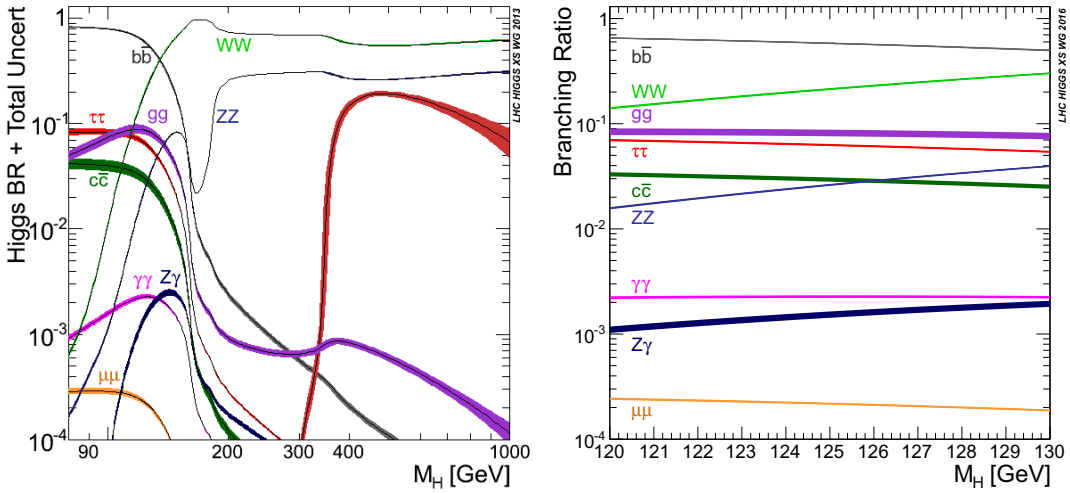

(a) (b)

Figure 4: Branching ratios for the decays of the SM Higgs boson (a) on a broad mass spectrum and (b) on a finer spectrum centered on 125 GeV

As can be noticed, the branching ratios (BR) vary in an appreciable manner and in a non-trivial way in the range of the Higgs' mass shown in Figure 4(a), producing very diverse final states topologies. For this very reason the search for the particle presented itself as a conundrum for physicists at accelerators, since at first its mass was unknown.

The top quark, being the heaviest fundamental particle, seems to be the preferable

decay channel for the Higgs (red line on the right in Figure 4(a)), however, if $M_H < 2m_t \simeq 350\ GeV$, the bottom quark one becomes dominant. Also note that the decay in $\tau^+\tau^-$ (the heaviest lepton) is one order of magnitude smaller than the $b\bar{b}$. Above kinematical thresholds of gauge bosons pair production (WW and $ZZ \simeq 200\ GeV$), the Higgs must decay mainly in this way; one notices also that (once above threshold) the BR of the WW decay is double that of ZZ. The photon is massless and for that reason it does not couple to the Higgs, however the decay $H \to \gamma\gamma$ is in fact possible through a boson loop (and in fact this will be of interest later in the present work); both Figures 4 show that the decay in two photons is much smaller than the one in bottom quarks for instance, nonetheless it is an important channel at the LHC, since two γs are a clear sign of the Higgs, especially in the low mass range.
Up to date calculations of branching ratios around the recently discovered mass of the Higgs boson, corresponding to Figure 4(b), can be found in [5].
The decay widths into massive gauge bosons $V = W, Z$ are proportional to the HVV couplings of (13), which can be written as:

$$\mathcal{L}_{HVV} = (\sqrt{2}G_\mu)^{1/2} M_V^2 H V_\mu V^\mu \tag{28}$$

these are s-wave coupling and even under parity and charge conjugation, corresponding to $J^{PC} = 0^{++}$ for the Higgs particle. For the case of the fermions, the decay widths are proportional to the $Hf\bar{f}$ couplings that are:

$$g_{Hff} \propto \frac{m_f}{v} = (\sqrt{2}G_\mu)^{1/2} m_f \tag{29}$$

Extensions of the SM predict an hypothetical CP-odd Higgs particle, which is generally denoted as A: in this case the coupling to gauge bosons is a p-wave corresponding to a particle sate $J^{PC} = 0^{+-}$; this last case will be further explored in the course of the thesis.

2.4 The discovery of the Higgs boson

The *Large Electron-Positron collider* (LEP) was inaugurated on the 14th of July of 1989 and it was the first accelerator that had reach into the potential mass range of the Higgs boson.
From 1989 to 2000, when the accelerator shut down,the four LEP experiments, ALPEH, DELPHI, L3 and OPAL collected data from e^+e^- collisions with an impressive performance. At such an e^+e^- collider, there were three important processes for the production of the Higgs: Z decay - $Z \to Hf\bar{f}$, in association with the Z - $e^+e^- \to Z + H$, and via WW or ZZ fusion - $e^+e^- \to \bar{\nu}H\nu, e^+He^-$.
The data obtained at both LEP-1 and LEP-2 phases made it possible for the first time to provide constraints on m_H, despite being relatively weak before the measurement of the top mass m_t in 1995, from when more accurate estimates were possible: values of $m_H < 300\ GeV$ were found during those initial times.
Thereafter, consecutive increases in the LEP center of mass energy during the LEP-2

phase that peaked in 2000 at 206 GeV led to the discovery of a few Higgs- like events near a mass of $\approx$ 115 GeV; unfortunately the decision was taken to shut down the accelerator in 2000, leaving a lower bound of 114 GeV at the 95% confidence level (CL).

After the shutdown of the LEP, the hadron collider *Tevatron* at Chicago,Illinois (the precursor of the famous *Large Hadron Collider* (LHC)) which operated from 1986 to 2011, took the lead of this seemingly elusive scientific endeavor. The CDF and D0 experiments at Tevatron, as the analyzed luminosity accumulated, excluded a range for the Higgs mass between 156 and 177 GeV, as well as a range of lower masses already excluded by the LEP.
Interestingly, before its closure in September 2011,the accelerator began to find a small excess of Higgs candidate events at the 160 GeV mark, though not strong enough to be considered evidence.

After a long period of construction, in 2008 the LHC and its detectors were ready to operate, and on September 10th of the same year the first beams were fired.
Just after 10 days following the inauguration, a first problem arose in the superconducting magnets which significantly damaged the accelerator and delayed the actual research of about 1 year, when it restarted at a center of mass energy of 7 GeV with a modest luminosity, which increased in 2011 anyway.

The Higgs bosons are extremely rare and in an hadron collider (where, contrary to an e^+e^- one, the main production channels are those reported in the previous section (26a) through (26d)), once signal-like events have been identified, statistical methods are made use of to quantify the significance of the said signals; stringent statistical requirements are in fact made: the significance of the signal is generally expressed as σ and in particle physics a significance of 3σ is regarded as evidence, while 5σ as an observation.

By the end of 2011, the ATLAS and CMS experiments had each accumulated and analyzed 5 fb^{-1} of data at a center of mass energy of 7 GeV. After combining all of the results, it was found that the SM Higgs boson appeared to be excluded for all masses except for a tiny interval around 125 GeV, where an excess of significance of around 3σ was found. These results were not "strong enough" to claim observation, and served to tighten the interval in which the Higgs mass was to be found.
In 2012 the center of mass energy was increased to 8 GeV, and in the summer of that very same year ATLAS had collected enough 5 fb^{-1} data to double its dataset: the significance of the small bump near 125 GeV was emphasized.

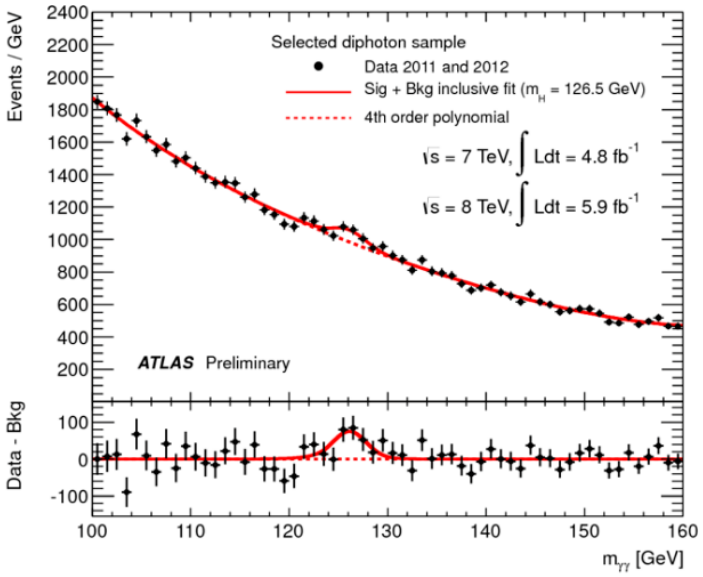

Figure 5: The plot of the invariant mass from pair of photons from the $H \to \gamma\gamma$ decay that was shown at the seminar at CERN on 4 July 2012. The excess of events over the prediction shown in red around 125 GeV is evidence of the sought for SM Higgs.

A joint seminar between ATLAS and CMS was announced at CERN for July 4 2012, where both the collaborations showed their founding of an excess of 5σ at a mass of 125 GeV.

After this incredible feat, researchers began to study the properties of the newly found particle to gauge its adherence to the predicted SM Higgs boson, and in fact it was first referred to as "Higgs-like" because the mass was the first and (at the time) only measured parameter out of many more that fully characterize the sought for particle.
In the SM, the Higgs boson is a spin-0 particle, it has no electric charge and it does not couple to gluons (i.e. it does not interact through the strong force); its spin and parity assignments were measured, as stated in the context of the decays of the Higgs, through the boson's decay properties. Amazingly all of the above properties, after they were measured, were found to be in agreement with the predicted ones.
Naturally it remains to be seen if the particle that was come across is the only Higgs boson or if it is one of many, such as those predicted by the supersymmetric model.
In the Standard Model, different couplings determine the Higgs' interaction with fermions and bosons, thus new physics might impact them differently. To summarize what is currently known about these interactions it is convenient to compare their coupling constants to the masses of the particles, as shown in the following figure:

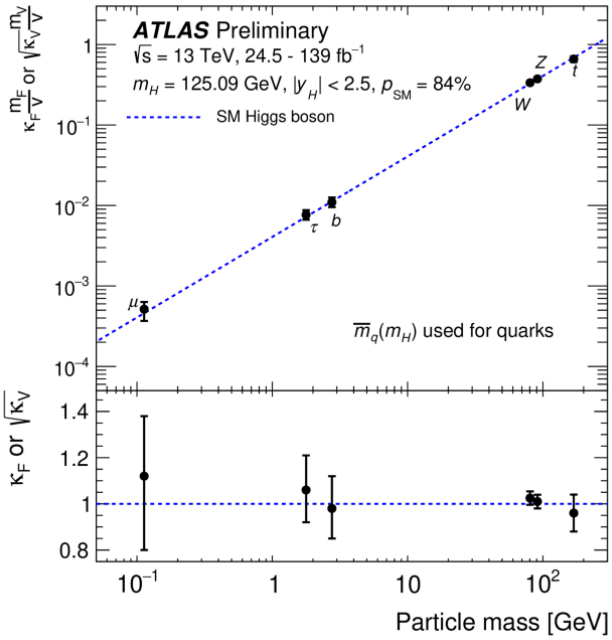

Figure 6: The measured coupling strength as a function of the mass of various particles in the Standard Model. Note that the mechanism through which fermion masses are generated is different from that concerning boson masses.

this shows that a particle's coupling strength depends on its very mass: the heavier the particle, the stronger the interaction, which is clearly a prediction of the Higgs mechanism in the Standard Model.
It is useful to keep in mind that weak bosons and fermion masses are generated through a conceptually different mechanism, and historically the Higgs-W/Z couplings were probed experimentally right after the discovery of the Higgs boson ([6] and [7]), whereas the Higgs-fermion ones only very recently, like in 2020 for the muon [8] and in 2018 for the third generation of fermions, top quark ([9] and [10]), bottom quark ([11] and [12]) and the tau lepton ([13] and [14]) . Indeed, the fact that fermion couplings to the Higgs were experimentally available only recently is part of the reason why the present thesis focuses on the study of the top-Higgs interaction.

A lot of questions still remain to be answered about the Higgs boson/mechanism. In 2024 a big step in performance will be brought by the *High-Luminosity LHC* (HL-LHC), which will increase by 10 the number of collisions and will consequently open the possibility to the study of the self-coupling of the Higgs: events produced via this channel feature two Higgs bosons in the final state, and are extremely rare. More general questions that will need to be answered concern, for instance, the fact that the MSSM, which could present ways to solve the riddle of dark matter, predicts that the mass of the Higgs should be less than $120 - 130\ GeV$; also of interest are the models that were recently proposed that maintain the Higgs to be the only link between regular and Dark Matter (DM), and whether all of the fermionic masses are in fact related to

the Higgs field, since we cannot explain why there would be such a hierarchy of the matter particles spanning from just a few eVs (neutrinos) up to the top quark, the heaviest fundamental particle.

3 Automated computation of cross sections at colliders

3.1 An overview of Feynman diagrams

The theoretical physicist Richard Feynman first introduced his now widely used diagrams in the late 1940s, as a bookkeeping device for simplifying calculations in an area of physics known to be very cumbersome: *Quantum-Electro-Dynamics* (QED), the quantum-dynamical study of electromagnetic forces, where lengthy and algebraically complicated calculations were quite often recurring.

Feynman famously introduced his diagrams in an invitation-only meeting at Pocono Manor Inn in rural Pennsylvania during the spring of 1948 to an audience of many theorists preoccupied with the problems brought on by QED. There were in fact two main problems with the calculations: for once, the theory produced unphysical infinities when pushed to higher orders of approximation (since, for instance in an interaction involving two electrons scattering off each other, the force-carrying virtual photons could borrow any amount of energy from the vacuum, even infinite, as long as they "paid it back" on a timescale dictated by the uncertainty principle), and the second problem was in regards to the formalism, which appeared to produce a large number of terms to keep track of and evaluate (in fact, even the simplest case of the interaction of two electrons was problematic, since the particles could exchange any number of photons, and all the possible interactions had to be accounted for), thus making it very difficult to use the theory.
This last problem was actually tamed by the theorists of the time by means of *perturbative* schemes, which enabled to approximate the full answer to a scattering process by keeping just those few terms that made the largest contribution since, as a general rule, the additional terms contributed insignificantly. In practice, this way of doing calculations was unfortunately extremely difficult, both because of the calculations themselves which involved divergences, and the fact that the terms present that were to be accounted for were still far too many.
The american physicist showed how some of the troublesome infinities could be removed (a trick now called *renormalization*) through the use of some mathematical tricks, some devised from scratch by himself, others borrowed; he also importantly used his diagrams to organize the process of the working out of a problem.
Feynman had in this way solved one of the most burdensome problems affecting theoretical physics at the time.

For various reasons the private meeting did not go well and the diagrams were made clear and popular at a later time thanks to the efforts of Feynman's younger associate Freeman Dyson.
In a few articles submitted to *Physical Review* Dyson showed the mathematical equivalence between Feynman diagrams and other methods introduced at the times by other physicists, such as Julian Schwinger and Tomonaga Sin-itiro, and derived the rules for

the diagrams' use (a kind of "how to" guide), including step by step instructions for the way they should be drawn and how they were supposed to be translated into the desired mathematical expressions; Dyson also showed that the troubling infinities in QED could be removed in a systematic way for all calculations, and not just for a few problems.

Soon Feynman diagrams gained followers throughout the fields of nuclear and particle physics and as such they were suddenly very helpful for collision events at the new accelerators, where they were primarily used to keep track of which particles participated in what types of interactions. Rules for making perturbative calculations of nuclear forces emerged in 1973, when H. David Politzer, David Gross and Frank Wilczek discovered the property of *asymptotic freedom* in QCD. Amazingly, other theorists adopted them for solving many-body problems in solid-state theory and by the end of the 1960s, some physicists even used versions of the drawings as an aid to solve gravitational physics.

The discoveries (and the interpretation of the results) of experiments such as the LHC and the underground ones concerning neutrino/dark matter physics, rely on the ability to make accurate predictions based on simulations. At the LHC, for instance, hadron collisions at such high energies produce final state topologies containing jets, heavy flavored quarks, leptons and what not, overwhelming the scientists with huge amounts of complicated data. There also could well be anomalies with respect to the SM predictions, leading to the necessity of having models that make *Beyond Standard Model* (BSM) physics predictions.
For these very reasons Monte-Carlo simulations appear to be not only necessary, but essential for the verification of predictions and the exploration of new theories.

General purpose matrix-element based event generators, such as CompHEP/CalcHEP, MadGraph5_aMC@NLO (which will be of particular interest), Sherpa and Whizard have been available for several years now.

3.2 Interaction theory and Feynman Rules

In theoretical particle physics a variety of different interactions occur, where generally a set of incoming particles interact with one another giving birth to a different set of outgoing particles.
For example, one such set of incoming particles can be an electron and a muon that, interacting with each other, produce a final state still composed of a muon and an electron:

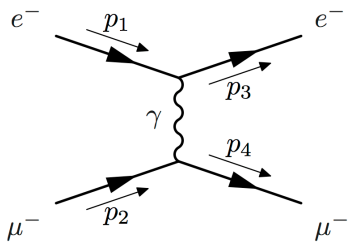

Figure 7: Illustrative Feynman diagram of the process $e^-\mu^- \to e^-\mu^-$, where the two particles interact by exchanging a virtual photon.

Another possibility is an electron and a positron coming together to form a muon and an anti-muon, or an incoming electron and a photon scattering off one another (Compton scattering) resulting in an outgoing electron and photon (with different momenta).
All of the above processes have each their own probability to occur, and the way physicists keep track of these is, in principle, the so called S-matrix (shorthand for "scattering matrix").
To illustrate the matrix's workings, following [15], we could consider an initial column vector for which each component represents a different initial eigenstate (two particle state as an example), as on the right-hand-side below:

$$\underbrace{\begin{bmatrix} e^-_{r^1,\mathbf{p}^1}, e^+_{r^2,\mathbf{p}^2} \\ e^-_{r^1,\mathbf{p}^1}, e^+_{r^2,\mathbf{p}^3} \\ e^-_{r^1,\mathbf{p}^2}, e^+_{r^2,\mathbf{p}^3} \\ \vdots \\ e^-_{r^2,\mathbf{p}^1}, e^+_{r^2,\mathbf{p}^2} \\ \vdots \\ e^-_{r^1,\mathbf{p}^1}, \gamma_{r^2,\mathbf{k}^1} \\ \vdots \end{bmatrix}}_{Final\ \ Eigenstates} = \underbrace{\begin{bmatrix} S_{11} & S_{12} & S_{13} & \dots & S_{1i} & \dots & \dots & \dots \\ S_{21} & S_{22} & S_{23} & \dots & S_{2i} & \dots & \dots & \dots \\ S_{31} & S_{32} & S_{33} & \dots & S_{3i} & \dots & \dots & \dots \\ \dots & \dots & \dots & \dots & \dots & \dots & \dots & \dots \\ S_{f1} & S_{f2} & S_{f3} & \dots & S_{fi} & \dots & \dots & \dots \\ \dots & \dots & \dots & \dots & \dots & \dots & \dots & \dots \\ \dots & \dots & \dots & \dots & \dots & \dots & \dots & \dots \\ \dots & \dots & \dots & \dots & \dots & \dots & \dots & \dots \end{bmatrix}}_{S-Matrix} \underbrace{\begin{bmatrix} e^-_{r^1,\mathbf{p}^1}, e^+_{r^2,\mathbf{p}^2} \\ e^-_{r^1,\mathbf{p}^1}, e^+_{r^2,\mathbf{p}^3} \\ e^-_{r^1,\mathbf{p}^2}, e^+_{r^2,\mathbf{p}^3} \\ \vdots \\ e^-_{r^2,\mathbf{p}^1}, e^+_{r^2,\mathbf{p}^2} \\ \vdots \\ e^-_{r^1,\mathbf{p}^1}, \gamma_{r^2,\mathbf{k}^1} \\ \vdots \end{bmatrix}}_{Initial\ \ Eigenstates} \tag{30}$$

that is related to the final eigenstate on the left-hand-side, where $\mathbf{p}$ and $\mathbf{k}$ indicate basis states of corresponding 3-momenta and r represents spin state for fermions and polarization state for photons.
The square of the absolute value of each component of the S-matrix gives the probability of an initial state i to transition to a final state f, for instance the probability that state 1 interacts and transforms into state 2 is given by:

$$S^*_{21}S_{21} = |S_{21}|^2 \tag{31}$$

In this way, each component of the S-matrix is a transition amplitude from a given initial state to a final eigenstate: the goal of particle physics is to calculate S_{fi} for any interaction, in other words to find a way to represent the matrix mathematically.

Equation (30) can be seen as an operator equation where an operator that we call "S-operator", or S_{oper} in short, changes an initial state $|i\rangle$ to a final state $|f\rangle$ with a probability S_{fi}:

$$S_{fi} = \langle f|S_{oper}|i\rangle \tag{32}$$

Clearly S_{oper} depends on the type of interactions taking place (electromagnetic, weak and strong ones) and there turns out to be a neat way of expressing it mathematically: given an interaction parametrized by the hamiltonian H_I^I (where the subscript I means that it is the interaction part of the full hamiltonian governing free fermion and boson fields, and the superscript means that we ar working in the interaction picture) the equation of motion for a ket state can be solved:

$$i\frac{d}{dt}\left|\psi(t)\right\rangle_I = H_I^I\left|\psi(t)\right\rangle_I \tag{33}$$

which, remembering that $\left|\psi(t_f)\right\rangle_I = S_{oper}\left|\psi(t_i)\right\rangle_I$, gives:

$$S_{oper} = exp(-i\int_{t_i}^{t} H_I^I\, dt') = exp(-i\int_{t_i}^{t_f}\int_V \mathcal{H}_I^I\, d^4x) \tag{34}$$

where V is the volume over which the interaction takes place, and $\mathcal{H}_I^I$ is the interaction hamiltonian density, that for the electromagnetic field (since it will be of importance later) is:

$$\mathcal{H}_{I,QED}^I = -e\bar{\psi}(x)\gamma^\mu A_\mu(x)\psi(x) \tag{35}$$

Thus, in principle, given H_I^I, through (32) we can find the desired transition amplitudes.
It turns out that the mathematics involved in calculating S_{oper} are made enormously simpler, instead of being almost intractable, by taking $V \to \infty$, and even though this assumption seems to not correlate to the real world (as particle/fields do not extend to infinity), results obtained by taking the said limit can be used to successfully predict the outcome of many scattering experiments. In physics one also considers the situation for which $t_i \to -\infty$ and $t_f \to \infty$, so that S_{oper} would have enough time to operate such that the final particle eigenstates are fixed, and no longer changing in time (this is sort of an "equilibrium" of final states). In this way we could define a new operator by the symbol S, which is the one that is usually employed in calculations:

$$S = S_{oper}(t_i \to -\infty, t_f \to +\infty, V \to +\infty) = exp(-i\int_{-\infty}^{+\infty} \mathcal{H}_I^I\, d^4x) \tag{36}$$

Now S_{oper} can be expanded:

$$\begin{aligned} S_{oper} &= \mathbb{I} - i\int_{t_i}^{t_f} H_I^I(t_1)\,dt_1 - \frac{1}{2!}T[(\int_{t_i}^{t_f} H_I^I(t_1)\,dt_1)(\int_{t_i}^{t_f} H_I^I(t_2)\,dt_2)] \\ &= \sum_{n=o}^{\infty}\frac{(-i)^n}{n!}\int_{t_i}^{t_f}\cdots\int_{t_i}^{t_f} T[H_I^I(t_1)H_I^I(t_2)...H_I^I(t_n)]\,dt_1dt_2...dt_n \end{aligned} \tag{37}$$

If the H_I^I above were just numeric functions of time, the order in which they are integrated with respect to t_n wouldn't matter at all, however since these terms are in fact operators (fields, as in (35)) that eventually act on a ket, the order is really important: the action of operators must occur in the same order as it occurs in nature, in time sequence, and the ordering is made with the time ordering operator T.
Thus, by (36):

$$S = \sum_{n=o}^{\infty}\frac{(-i)^n}{n!}\int_{-\infty}^{+\infty}\cdots\int_{-\infty}^{+\infty} T[\mathcal{H}_I^I(t_1)\mathcal{H}_I^I(t_2)...\mathcal{H}_I^I(t_n)]\,d^4x_1d^4x_2...d^4x_n \tag{38}$$

Our first goal is to describe leptons interacting electrically with each other, so the next step would be top plug (35) in (37) and basically develop QED, a process which gives a hint as to the absolute necessity of Feynman diagrams:

$$\begin{aligned} S &= \underbrace{\mathbb{1}}_{S^{(0)}} + \underbrace{ie\int_{-\infty}^{+\infty}(\bar{\psi}\not{A}\psi)_{x_1}\,d^4x_1}_{S^{(1)}} + \underbrace{\frac{(-i)^2e^2}{2}\int_{-\infty}^{+\infty}\int_{-\infty}^{+\infty} T[(\bar{\psi}\not{A}\psi)_{x_1}(\bar{\psi}\not{A}\psi)_{x_2}]\,d^4x_1d^4x_2}_{S^{(2)}} + ... \\ &= \sum_{n=0}^{\infty} S^{(n)} \end{aligned} \tag{39}$$

Calculating at the necessary order the terms in (39) would give us the amplitude for any given process we might like. For example the $S^{(1)}$ term comprises 8 subterms (expanding the first integral in (39)) which describe processes that involve just one interaction ("single vertex interactions") between the particles, and it turns out that in QED all these terms are zero, which means that the theory does not allow for single vertex processes.
$S^{(2)}$ on the other hand gives rise to a large number of terms that describe processes involving two interactions in total ("two vertices interactions"), such as two leptons interacting through a virtual photon (the process analyzed below), Compton scattering, electron/positron closed loop diagrams and so on. In general the term $S^{(n)}$ gives the amplitude for a process involving n vertices, which can be a new process on its own, or just a correction to one.
It is very interesting and life saving to note that each $S^{(n)}$ has a factor e^n in front, and in natural units ($\hbar = c = 1$) it is known that:

$$\alpha = \frac{e^2}{4\pi} \approx \frac{1}{137} \quad \rightarrow \quad e \approx \sqrt{\frac{4\pi}{137}} \approx .303 \tag{40}$$

Hence in (39) each term has a dimensionless factor of $\approx (.303)^n$ in front, so that higher orders are suppressed and in QFT considered as corrections to the leading terms, which means, for instance, that the leading order amplitude calculation of two electrons scattering off each other will be $S^{(2)}$, and higher order calculations with higher powers of e will just give corrections to the amplitude.

Expanding each term in (39) would require some seriously and tediously long algebraic calculations, therefore Feynman devised a set of rules, the so called "Feynman rules", that allow to simply write down the transition amplitude for a given process by looking at its associated Feynman diagram. The rules themselves apply to what are termed "topologically different Feynman Diagrams", which are different from one another in ways other than simply changing the labeling of the vertices. Feynman diagrams are usually represented by drawings where the time axis is usually (but not exclusively) directed vertically, fermions are represented by a straight line (which represents their momentum) pointing to the right, anti-fermions by a straight line pointing to the left and photons by a squiggly line:

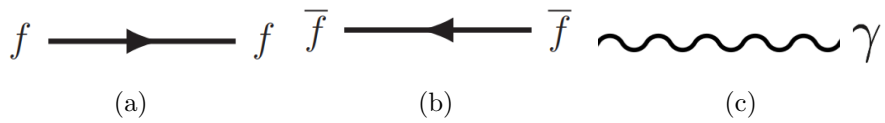

Figure 8: Constituents of a QED Feynman diagram: (a) a fermion, (b) an anti-fermion and (c) a photon.

Feynman's rules, for electrons and positrons in QED are:

1. The S-matrix element for a given interaction is:

$$S_{fi} = \delta_{fi} + ((2\pi)^4 \delta^{(4)}(P_f - P_i)(\prod_{\substack{all\ external \\ bosons}} \sqrt{\frac{1}{2V\omega_{\mathbf{k}}}})(\prod_{\substack{all\ external \\ fermions}} \sqrt{\frac{m}{VE_{\mathbf{P}}}}))\mathcal{M}$$
$$\mathcal{M} = \sum_{n=1}^{\infty} \mathcal{M}^{(\backslash)} \tag{41}$$

   where P_f is the total 4-momentum of all final particles, P_i is the total 4-momentum of all initial particles and $M^{(n)}$ comes from the contribution of the nth order perturbation term $S^{(n)}$.

2. The amplitude $M^{(n)}$ is obtained from all of the topologically distinct, connected Feynman diagrams which contain n vertices. The contribution to each $M^{(n)}$ is obtained by the following procedure:

3. For each vertex, include a factor of $ie\gamma^{\mu}$.

4. For each internal photon line, labeled by 4-momentum k, include a factor $iD_{F\mu\nu}(k) = i\frac{-g_{\mu\nu}}{k^2+i\epsilon}$

5. For each internal fermion line, labeled by 4-momentum p, write a factor $iS_F(p) = i\frac{\not{p}+m}{p^2-m^2+i\epsilon}$.

6. For each external line, write one of the following spinor factors:
   a) for each initial electron: $u_r(\mathbf{p}$
   b) for each final electron : $\bar{u}_r(\mathbf{p})$
   c) for each initial positron : $\bar{\nu}_r(\mathbf{p})$
   d) for each final positron : $\nu_r(\mathbf{p})$
   e) for each initial photon : $\epsilon_{r,\mu}(\mathbf{k})$
   d) for each final photon : $\epsilon_{r,\mu}(\mathbf{k})$

7. The spinor factors (γ matrices, S_F functions, spinors) for each fermion line are written in order so that, reading from left to right, they occur in the same sequence as following the fermion line in the direction of its arrows through the vertex.

8. The 4-momenta at each vertex are conserved.

9. For each closed loop of internal fermions only, take the trace in spinor space of the resulting matrix and multiply by a factor of (-1).

10. For each 4-momentum q which is not fixed by 4-momentum conservation, carry out the integration $\frac{1}{(2\pi)^4}\int d^4q$. One such integration for each closed loop.

11. Each interchange of neighboring fermion operators, which is required to place the expression in appropriate normal order, carries with itself a factor of (-1).

A straight forward application of those rules would be the interaction where both initial and final states are composed of an electron and a positron.
Since the only measurable quantity in an experiment are the external lines, i.e. the particles entering and exiting into or from the scattering volume, at the leading order (e^2) there are two (indistinguishable, in the said sense) ways in which this interaction can occur: either there is an annihilation of e^+ with e^-, followed by a creation of the same two types of particles, or one of the incoming particles emits a virtual photon which is then absorbed by the other particle:

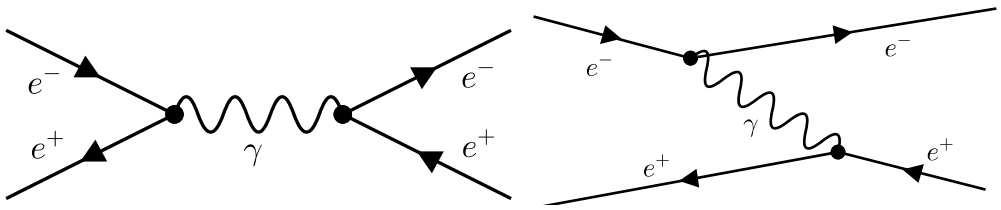

Figure 9: Two types of ways in which the interaction $e^+e^- \to e^+e^-$ can happen.

For the diagram on the left, following the fermion arrows for incoming particles, we place the electron spinor $u_r(\mathbf{p})$ on the far right and to its left an $ie\gamma^\mu$ matrix factor, representing the left vertex, finally on the far left we place the positron spinor $\bar{\nu}_r(\mathbf{p})$:

$$\bar{\nu}_{r_2}(\mathbf{p}_2) ie\gamma^\mu u_{r_1}(\mathbf{p}_1) \tag{42}$$

As a sidenote, in the above expression spinor indices are hidden, but they are the reason why the order of spinors placement is important.
To the left of (42), as the rule 2) imposes, we place a photon propagator in momentum space followed by the spinors for the final particles:

$$\mathcal{M}^{(2)}_{LH} = \bar{u}_{r'_1}(\mathbf{p}'_1) ie\gamma^\mu \nu_{r'_2}(\mathbf{p}'_2) iD_{\mu\nu}(k = p_2 + p_1) \bar{\nu}_{r_2}(\mathbf{p}_2) ie\gamma^\mu u_{r_1}(\mathbf{p}_1) \tag{43}$$

where LH stands for Left-Hand (side, of Figure 9), and the superscript (2) because that is the leading order, as specified above.
The final step is to use (41):

$$\begin{aligned} S^{(2)}_{LH} = (\prod_{\substack{all\ external \\ fermions}} \sqrt{\frac{m}{VE_{\mathbf{P}}}})((2\pi)^4 \delta^{(4)}(p_1 + p_2 - (p'_1 + p'_2)) \times \\ \bar{u}_{r'_1}(\mathbf{p}'_1) ie\gamma^\mu \nu_{r'_2}(\mathbf{p}'_2) iD_{\mu\nu}(k = p_2 + p_1) \bar{\nu}_{r_2}(\mathbf{p}_2) ie\gamma^\mu u_{r_1}(\mathbf{p}_1) \end{aligned} \tag{44}$$

which is the correct amplitude if one were to do the actual calculation with the integral of time ordered operators (39).
For the right diagram in Figure 9, if we follow the same steps, the first vertex reads:

$$\bar{u}_{r'_1}(\mathbf{p}'_1) ie\gamma^\mu u_{r_1}(\mathbf{p}_1) \tag{45}$$

then we include the propagator and the second vertex terms, all of which yield:

$$\mathcal{M}^{(2)}_{RH} = -\bar{\nu}_{r_2}(\mathbf{p}_2) ie\gamma^\mu \nu_{r'_2}(\mathbf{p}'_2) iD_{\mu\nu}(p_2 - p'_2) \bar{u}_{r'_1}(\mathbf{p}'_1) ie\gamma^\mu u_{r_1}(\mathbf{p}_1) \tag{46}$$

where a factor of $(-1)^3$ had to be included because operator associated with the $\bar{u}$ spinor was moved leftward past the two other operators, followed by the fact that the operator $\bar{\nu}$ was moved to the right past one operator, to obtain the same order as (43). Therefore, gluing all the amplitudes together, we find the following:

$$S^{(2)} = S^{(2)}_{LH} + S^{(2)}_{RH} = (\prod_{\substack{all\ external\\ fermions}} \sqrt{\frac{m}{VE_{\mathbf{P}}}})((2\pi)^4\delta^{(4)}(p_1 + p_2 - (p'_1 + p'_2))(\mathcal{M}^{(2)}_{LH} + \mathcal{M}^{(2)}_{RH}) \tag{47}$$

which indeed saved us from a flood of algebraic calculations.

Feynman rules were illustrated only for positrons and electrons, but they can be easily generalized to include all three generations of leptons, since the Feynman amplitude for a given process can be calculated by assuming that all leptons are electrons/positrons and then replacing the spinors and/or propagators with those representing the actual other flavors, so that the only difference in form of the results will be the masses of the fermions.

This S-matrix/operator formalism is in fact very important as it allows to calculate differential cross section of scattering processes using the Fermi golden rule:

$$d\sigma = \frac{1}{2s}|\mathcal{M}|^2\, dPS \tag{48}$$

where the s variable is the squared center of mass energy of the process, thus for two particles colliding with four-momenta p^i would be $s = (p^1 + p^2)^2$, $\mathcal{M}$ is to be found in (41) with Feynman rules (like we did with electron scattering above) where every term proportional to e^n is naturally to be considered, and dPS is the Lorentz invariant phase-space integration factor which is given by (for $2 \to n$ scatterings where the final state consists of n particles):

$$dPS(\overbrace{P}^{Initial\ State}, \overbrace{p'^1, ..., p'^n}^{Final\ State}) = (2\pi)^4\delta^{(4)}(P - (p'^1 + ... + p'^n)) \prod_{\substack{all\ external\\ particles}} \frac{d^3p'_j}{(2\pi)^3 E_j} \tag{48}$$

where $P = p^1 + p^2$.

As remarked above, this formalism began to involve very different areas of physics including (and especially for the present work) QCD with the discovery of asymptotic freedom in 1973; QCD describes the interactions between colored particles mediated by (the also colored) gluons, where the strength of the interaction is not (40) anymore but is set by the 'strong' coupling constant. Feynman rules for the said theory will not be discussed here but the same process to extract them as for QED above applies, although it requires a bit more effort.

It is worth mentioning that although the calculations involved for the computation of analytic cross sections seem to be quite of a mechanic nature, as displayed in the example above, for $2 \to n$ scatterings the terms involved rapidly increase in number

and one has to resort to numeric methods, such as the one described in the following section.

3.3 Automating cross section calculations

MadGraph5_aMC@NLO [16] is a tool that automates the generation of matrix elements for high energy physics processes, such as decays and $2 \to n$ scatterings.

To use the program, first the user specifies the desired process in terms of the initial and final states' particles, including various refined criteria (forced resonances, excluded internal particles, forced decay chains of final particles). Of help are multiparticle labels that can be used to probe all possible processes involving a vast range of particles.
Once the sought for model is specified by the user, MadGraph generates all Feynman diagrams for the processes and outputs the code necessary to evaluate the matrix element (amplitude) at a given phase space point. The algorithm to generate the diagrams (and thus the code) is based on recursively generating sub-diagrams from the diagrams by merging legs with the addition of a flag `from_group`, to help indicate whether a given particle results from a merging of particles in the previous step (`True`) or if it is simply copied from the previous step (`False`); the flag massively helps to ensure not to double-count diagrams.
The steps of the algorithm are:

1. Given the model (initial and final state particles the user selects), generate two hash maps containing information about the interactions in the model. The first one (called `Vertices`) maps all combinations of n particles to all n-point interactions combining the particles, and maps all pairs particle-antiparticle to "0". The second dictionary (called `Currents`) maps, for all $n-$point interactions, $n-1$ particles to all combinations of resulting particles for the interactions.

2. Flip particle/anti particle status for incoming particles in the process. Set the flag `from_group` = `True` for all external particles

3. If there is an entry in the `Vertices` dictionary combining all external particles, create the combination $[(1, 2, 3, 4, ...)]$ if at least two particles have `from_group` = `True`.

4. Create all allowed groupings of particles with at least one `from_group` = `True` present in the `Currents` dictionary.

5. Set `from_group` = `True` for the newly combined particles, and `False` for any particle that has not been combined in this iteration. Repeat from 3 for the reduced set of external particles.

6. Stop algorithm when at most 2 external particles remain.

Once the code is generated by MadGraph in the said way, the evaluation of the matrix element at a given phase space point is carried out in terms of successive calls to a helicity amplitude function library (in MadGraph either HELAS or ALOHA). For each external leg in the generated diagram a helicity wavefunction is created, then they are all combined into new wavefunctions corresponding to the propagators in the diagrams. The final vertex corresponds to a helicity amplitude call which returns the value of the amplitude corresponding to the diagram.
MadGraph also produces pictorial representations of the Feynman diagrams for the process that is being analyzed.

Importantly, the matrix element code generated can be used to calculate cross sections or decay widths and for event generation, generally with the aid of a package like MadEvent [17], which is included in MadGraph5_aMC@NLO.
The calculation of cross sections is normally not a trivial task, in fact the number of subprocesses contributing to a process can be fairly large, and the complexity of each subprocess grows very quickly in relation to the number of final state particles.
The integration of the squared amplitude (generated in the first steps, as discussed above) over the phase space is necessarily performed with Monte Carlo techniques, which need to solve for various problems, one of which being the fact that the amplitude is most of the times a very complicated function of the momenta and exhibits sharp peaks, thus one needs to identify their location and map them onto several other sets of variables ("channels") to achieve an efficient numerical integration. Fortunately, a standard Feynman diagram expansion gives the said information on the position and shape of the peaks.
To summarize this process, the user specifies a process for which MadGraph first generates the amplitudes for each of the relevant subprocesses, and then produces the mappings for the integration over the phase space.
This information is afterwards passed on to MadEvent, which produces a stand-alone code that allows the user to calculate cross sections.

MadGraph5_aMC@NLO can be either used directly online on the web or locally. The code can be downloaded from the web page `https://launchpad.net/madgraph5`. The user can start the command line interface by running `bin/mg5` from the MadGraph directory.
As an illustrative example of the program, consider the evaluation of the cross section for top-pair production in the SM: syntax as easy as follows needs to be used

```
generate p p > t t~ QED=2 QCD=2
output my_dir
launch
```

(where the commands `QED=2 QCD=2` serve to specify the order of the diagram, and the tilde indicates the anti-particle) to get the results:

Results in the sm for p p > t t~ QED=2 QCD=2

Available Results

Run	Collider	Banner	Cross section (pb)	Events	Data	Output	Action
run_01	p p 6500.0 x 6500.0 GeV	tag_1	505.8 ± 0.93	10000	parton madevent	LHE plots	remove run | launch detector simulation

Main Page

Figure 10: Online results of total cross section for the process $pp \to tt\tilde{}$ at a center of mass energy of $6500 + 6500\ GeV$.

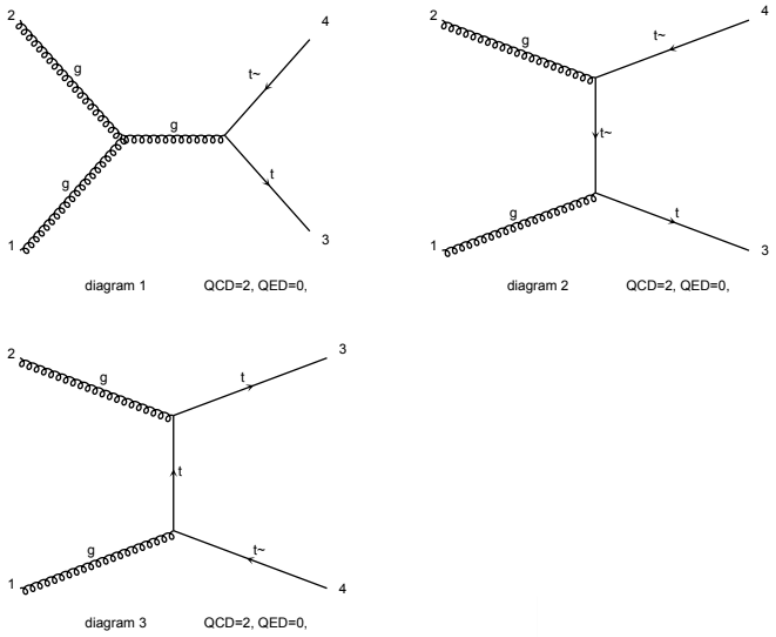

Figure 11: Feynman diagrams created by MadGraph5_aMC@NLO for the process considered. These are 3 of the 15 diagrams of all the subprocesses.

Finally, note that we introduced the basic concepts of MadGraph, however for more complicated processes (like BSM physics, decay chains, NLO calculations) one needs to resort to advanced tools that are beyond the scope of the present work, for which we refer the reader to the *References*.

4 Constraints on the Higgs-top interaction from various channels

4.1 Parametrizing the interaction

The existence of a new boson with a mass of 125 GeV is at the present moment certain through the accumulation of a huge amount of evidence.
Making sure that the particle is in fact the one predicted by the Standard Model is one of science's most important tasks, as it would imply the necessary evidence in support of the Higgs mechanism, the discovery of the first fundamental spin-0 particle and finally the existence of a new short-range interaction, different from the known ones, of a Yukawa-type.
The top-quark Yukawa interaction, due to its strength, has naturally played a central and fundamental role in the discovery of the said scalar particle, and the combination of various measurements has provided evidence that the strength of the interaction is in agreement with the SM expectations, as can be seen in Figure 6. While improving the precision of the measurement of the strength of top-Higgs interaction was quite straight forward, probing the structure and properties of it was (and still in part is) considerably more of an open question. In fact, a way to assess whether the newly found boson is actually the SM one is to consider the CP properties of the top-Higgs coupling, i.e. if the Higgs couples to scalar (SM case), pseudoscalar or both fermion densities, which is basically the goal of the present work. Gathering data on the CP properties of the top quark Yukawa interaction is a highly non-trivial task, since there is no decay mode to or through top quarks of the Higgs that can be studied (Figure 4(a) and 4(b)), and thus only Higgs production is to be contemplated.
The approach is based on an effective field theory (EFT) valid up to a scale Λ below the electroweak symmetry breaking (EWSB) scale (where $SU(2)_L \times U(1)_Y$ reduces to $U(1)_Q$) that features only one new state $X(J^P) = 0^+, 0^-$, where other spins have been excluded by early experimental works (see for instance [18]), and it is assumed that any other new state is to be found at scales larger than Λ, since no BSM evidence has been summoned by the present data; furthermore, and more to the point of this thesis, we do not require CP conservation (in the Higgs sector), and we leave the possibility open for the new state to have no definite CP properties. The effective interaction Lagrangian relevant for the top quark is eq. (2.2) in [19]:

$$\mathcal{L}_0^t = -\bar{\psi}_t(c_\alpha k_{Htt} g_{Htt} + i s_\alpha k_{Att} g_{Att} \gamma_5)\psi_t X_0 \tag{49}$$

where X_0 labels the new 125 GeV particle, $c_\alpha \equiv cos(\alpha)$ and $s_\alpha \equiv sin(\alpha)$ are CP mixing parameters, k_{Htt} and k_{Att} are dimensionless real coupling parameters and $g_{Htt} = g_{Att} = \frac{m_t}{v} = \frac{y_t}{\sqrt{2}}$, with $v \sim 246\ GeV$.
The parametrization (49) has the practical advantage of being able to interpolate continuously one scenario to the other, for example the SM scenario (see (17)) is recovered by setting $\alpha = 0$, $\alpha = \pi/2$ corresponds to the Higgs being a pure pseudoscalar state and the state $\alpha = \pi$ is the SM case with a flipped interaction constant.

Note that the top Yukawa interaction induces effective couplings between vector bosons and the Higgs, that can be parametrized by eq (2.4) in [19], which will not be shown here; also to note is that these Higgs-vector bosons interactions will remain SM-like (no new physics in these couplings is hypothesized), since they have been studied for a long time and are thus known to a higher degree of precision.
The implementation of the Lagrangian (49) in MadGraph5_aMC@NLO is done through the *Higgs Characterization model* (HC) publicly available online [1], which will be used in this work.
To summarize, the aim of this thesis is to probe the Higgs-top Yukawa coupling by means of different processes to determine, through the use of recent experimental results, whether the newly found scalar resonance is in fact the predicted SM one. To this end we use the parametrization (49) which allows to interpolate between scenarios very rapidly and with relative ease.
The processes will be considered at LO and they are: Higgs production with a pair of top quarks (26(d)) ($t\bar{t}H$), Higgs production in association with a single top quark (tH) and multi-top production ($t\bar{t}t\bar{t}$). Also the same effective theory will be used in analyzing the scalar/pseudoscalar state through other processes such as gluon fusion ((26(a)))(ggH) and the Higgs' decay into two photons ($H \to \gamma\gamma$); for these last two processes the cross section and the branching ratio are known analytically and numeric integration will not be required. Combining the results of all these processes, we will show that the phase of the top-quark Yukawa coupling can be bounded at the current $\sim 137\ fb^{-1}$ luminosity of the LHC, and predictions for later runs with higher luminosities, $300\ fb^{-1}$ (roughly the luminosity that will be achieved at the end of Run 3 at the LHC) and $3000\ fb^{-1}$ (approximate luminosity at the HL-LHC), will put an even more stringent bound on the coupling.

4.2 Results

The first channel that is analyzed is Higgs production in association with a top-quark pair, which was well illustrated and expanded on above; we follow the general thread in [20]. The code and events for $t\bar{t}X_0$ hadroproduction can be generated at LO in MadGraph using the following code:

```
import model HC_NLO_X0
generate p p > x0 t t~
output
launch
```

and the representative Feynman diagrams for the said process are, other than Figure 2(d):

[1] http://feynrules.irmp.ucl.ac.be/wiki/HiggsCharacterisation

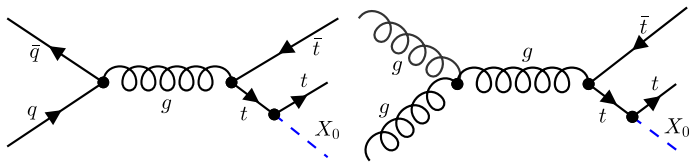

(a) (b)

Figure 12: Illustrative Feynman diagrams for $t\bar{t}H$ production.

It is worth noting that, since in every diagram the Higgs couples to the top quark, the cross section cannot be sensitive to the sign of the Yukawa coupling y_t and in fact $\sigma \sim y_t^2$, thus the SM cross section is also compatible with a "flipped sign" state (basically the SM with the coupling constant being $-y_t$, which corresponds to $\alpha = \pi$ in (49)). The following figure exhibits this behavior very well:

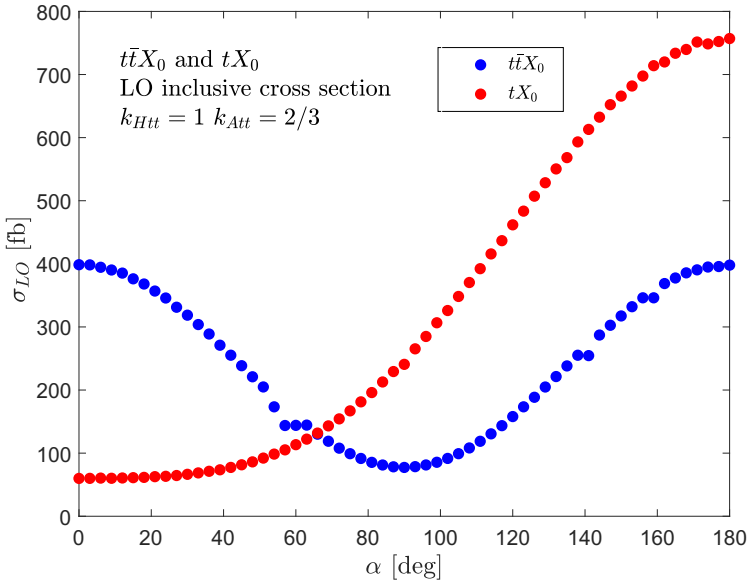

Figure 13: LO inclusive cross section for both the $t\bar{t}X_0$ and tX_0 channel. The blue curve is symmetric with respect to $\alpha = 90°$ as expected, whereas the red one depends on the sign of y_t.

instead the single top quark production (which will be of importance in a moment) is heavily dependent on the sign of y_t.
We rewrite the parametrization (49) in a handier way:

$$\mathcal{L}_0^t = -\frac{m_t}{v} X_0 \bar{\psi}_t (a_t + i b_t \gamma_5) \psi_t \tag{50}$$

with the clear identification:

$$a_t = cos(\alpha) k_{Htt} \quad \text{and} \quad b_t = sin(\alpha) k_{Att} \tag{51}$$

As a consequence the total cross section will have term proportional a_t^2, another to b_t^2 and a term linear in $a_t b_t$.
We simulate events at center-of-mass energy of $\sqrt{s} = 13\ TeV$, set the resonance mass $m(X_0)$ to 125 GeV and the top mass to 173 GeV and finally use $k_{Htt} = 1$, $k_{Att} = 2/3$ (to recover the SM gluon fusion cross section in the limit $m_t \to \infty$, which is a very good approximation for Higgs masses in the $120 - 130\ GeV$ range).
We obtain the following parametrization for the total cross section:

$$\sigma(t\bar{t}H)_{13\ TeV} = 408.6a_t^2 + 78.47b_t^2 - 0.206a_t b_t \tag{52}$$

Recent results [21] show that the ratio between the experimental and the SM cross section is, at 137 fb^{-1}:

$$\mu_{t\bar{t}H}^{Exp} = 0.92 \pm 0.19(\text{stat})^{+0.17}_{-0.13}(\text{syst}) \tag{53}$$

whereas theorically, we assume that at 300 fb^{-1} and 3000 fb^{-1} the ratio is 1 and the uncertainties scale as the square root of the luminosity:

$$\mu_{t\bar{t}H}^{300} = 1^{+0.17}_{-0.15} \quad \mu_{t\bar{t}H}^{3000} = 1^{+0.05}_{-0.05} \tag{54}$$

It is important to note that throughout all the results, we assume that there are no theoretical uncertainties (i.e. on numerical predictions) and thus we only consider the statistical ones. Also we ignore systematical uncertainties, in the sense that we assume they also scale with the square root of the luminosity, as can be seen in (54). Using (53) and (54), at the 1σ CL we get bounds on the parameters a_t and b_t:

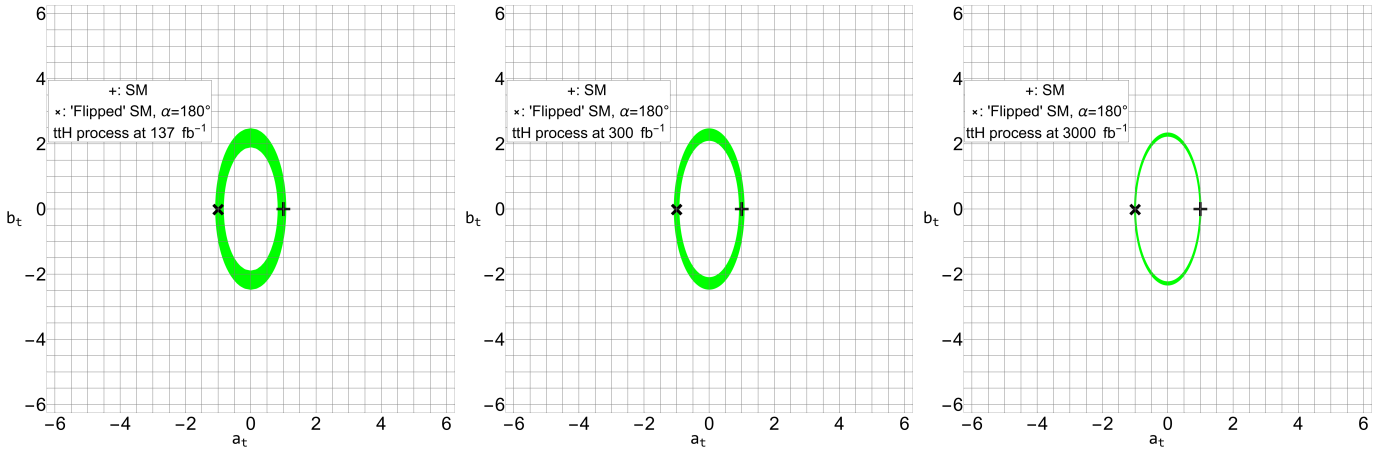

(a) (b) (c)

Figure 14: Parameter space consistent at the 1σ CL with (a) the measurement at 137 fb^{-1} of the $t\bar{t}H$ process inclusive LO cross section, (b) the prediction at 300 fb^{-1} and (c) at 3000 fb^{-1} involving no new physics. The upright cross represents the SM and the slanted one is the 'Flipped' SM ($-y_t$).

The channel we consider next is the Higgs production in association with a single top-quark, for which we follow the work done in [22].
At LO in QCD one can generally divide the process in question into three main groups, depending on the virtuality of the W boson (that partakes of the interaction): t-channel and s-channel feature respectively a space-like and a time-like W, whereas associated production with a W boson features an on- shell W; in fact tH production is always mediated by a tWb vertex and this implies the existence of a b quark either in the initial (t-channel and associated W production) or final (s-channel) state. This subdivision into three categories is generally an approximation that holds together until NLO, where the processes start interfering with each other.
The single top associated production is characterized by a smaller cross section than the main Higgs production channels, however it resides in a rather small class of channels that are sensitive to the sign of the top Yukawa coupling, as was shown above in Figure 13, in fact for t-channel and W associated production, the diagrams that feature a coupling of the W with the top interfere destructively with the ones in which the Higgs couples to the W, making cross sections very sensitive to potential deviations from the SM.
In this thesis we are mainly interested in the t-channel process, which in MadGraph5_aMC@NLO is obtained with:

```
import model HC_NLO_X0-no_b_mass
define p = p b b~
define j = p
generate p p > x0 t j $$ w+ w-
add process p p > x0 t~j $$ w+ w-
output
launch
```

where the `$$ w- w-` syntax removes s-channel as well as associated W production from tH production, and `no_b_mass` sets the bottom quark's mass to zero.
The relevant LO Feynman diagrams are:

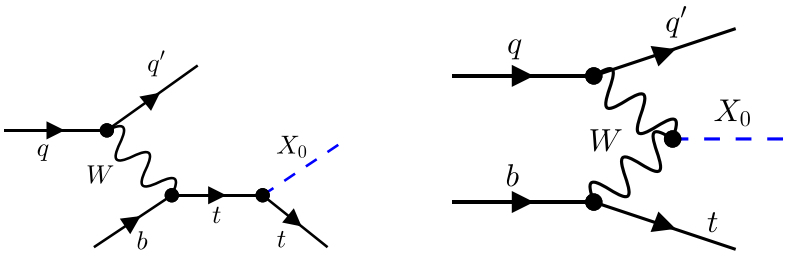

Figure 15: Illustrative Feynman diagrams for t-channel tH associated production.

For the numerical calculation we set the mass of the resonance $m(X_0)$ to 125 GeV, the top mass to 173 GeV, $k_{Htt} = 1$, $k_{Att} = 2/3$ and generate events at a center of mass

energy of $\sqrt{s} = 13\ TeV$. It is also worth noting that in Figure 15 the Higgs also couples to the W for which, referring to eq. (2.4) in [19], we use the boundary condition:

$$k_{SM} \cdot c_\alpha = 1 \tag{55}$$

since we want this interaction to remain in the SM.
Taking into account the diagrams in Figure 15, we find the inclusive LO cross section for the tH process to be parametrized by:

$$\sigma(tH)_{13\ TeV} = 221.03 + 200.74a_t^2 + 27.5b_t^2 - 325.95a_t + 0.054b_t \tag{56}$$

where the first three terms are the total cross sections of the single diagrams, whereas the last two are interference terms, and we have neglected the mixing term proportional to $a_t b_t$ as its contribution is about an order of magnitude less than the cross section $\propto b_t$.
Recent measurements [21] have reported a ratio between the experimental cross section and the SM one at 137 fb^{-1} to be:

$$\mu_{tH}^{Exp} = 5.7 \pm 2.7(\text{stat}) \pm 3.0(\text{syst}) \tag{57}$$

whereas, using the same arguments as before, we use the following ratios for the 300 fb^{-1} and 3000 fb^{-1} runs:

$$\mu_{tH}^{300} = 1^{+2.73}_{-1} \quad \mu_{tH}^{3000} = 1 \pm 0.86 \tag{58}$$

where in 300 fb^{-1} we have prevented the ratio from becoming negative, since (56) renders it impossible. Using (57) and (58), at the 1σ CL we get bounds on the parameters a_t and b_t:

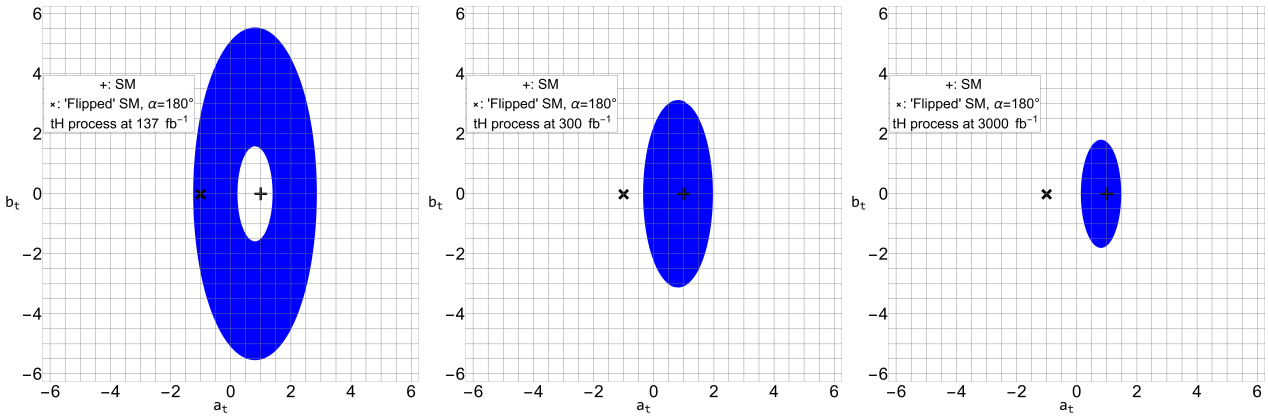

(a) (b) (c)

Figure 16: Parameter space consistent at the 1σ CL with (a) the measurement at 137 fb^{-1} of the tH process inclusive LO cross section, (b) the prediction at 300 fb^{-1} and (c) at 3000 fb^{-1} involving no new physics. The upright cross represents the SM and the slanted one is the 'Flipped' SM ($-y_t$).

It is worth noting already that in Figure 16(a) the Standard Model coupling is not contained within 1σ , however this channel is notoriously hard to measure at the LHC, leading to highly imprecise results of the type (57). Also, as was just said above, since the diagrams that contain the top interfere with the ones involving weak bosons, the cross section (56) includes a term linear in a_t (and b_t) which reflects itself in the fact that the allowed region in Figure 16 is not centered in the origin, but is shifted.

The third process analyzed regards the production of 4 top quarks ($\bar{t}t\bar{t}t$ production), for which we follow the works [23] and [24].
The code to generate LO $t\bar{t}t\bar{t}$ production is the following:

```
import model HC_NLO_X0
generate p p > t t~t t~
output
launch
```

This process can occur either through gluon mediation, electroweak gauge-boson mediation or Higgs boson mediation. The representative Feynman diagrams for these channels are:

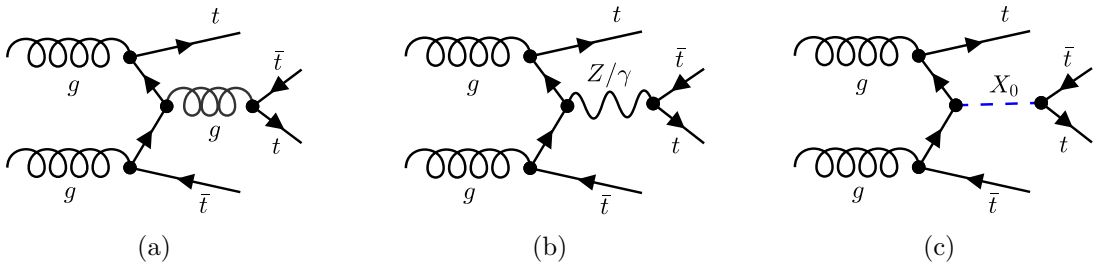

Figure 17: Illustrative Feynman diagrams for $t\bar{t}t\bar{t}$ production mediated by (a) a gluon (b) an electroweak gauge-boson and (c) the Higgs boson.

For the above Feynman diagrams we name the corresponding matrix element contributions (as in [24]): $\mathcal{M}_g$ for figure 17(a), $\mathcal{M}_{Z/\gamma}$ for (b) and $\mathcal{M}_X$ for (c), giving a total cross section of:

$$\sigma(t\bar{t}t\bar{t}) = \sigma(t\bar{t}t\bar{t})_{g+Z/\gamma} + \sigma(t\bar{t}t\bar{t})_{int} + \sigma(t\bar{t}t\bar{t})_X \tag{59}$$

where

$$\begin{aligned} \sigma(t\bar{t}t\bar{t})_{g+Z/\gamma} &\propto \left|\mathcal{M}_g + \mathcal{M}_{Z/\gamma}\right|^2 \\ \sigma(t\bar{t}t\bar{t})_{int} &\propto \mathcal{M}_{g+Z/\gamma}\mathcal{M}_X^\dagger + \mathcal{M}_{g+Z/\gamma}^\dagger\mathcal{M}_X \\ \sigma(t\bar{t}t\bar{t})_X &\propto \left|\mathcal{M}_X\right|^2 \end{aligned} \tag{60}$$

Note that this line of reasoning should be followed even in processes like $t\bar{t}H$ where one can imagine a channel like $qq \to W/\gamma \to t\bar{t}H$, that however is expected to be

suppressed due to the amount of EW interactions as compared to Figure 2(d), and in fact one finds this to be correct. In this respect 4-top production is an outlier, in the sense that EW contributions violate those kind of reasonings; also, were we not to involve EW contributions, the process would not be sensitive to the top Yukawa coupling.
We thus calculate the terms in (60) numerically setting the mass of the resonance $m(X_0)$ to 125 GeV, the top mass to 173 GeV and we generate events at a center of mass energy of $\sqrt{s} = 13\ TeV$. We obtain the following cross section:

$$\sigma(t\bar{t}t\bar{t})_{13\ TeV} = 9.975 + 1.136a_t^4 + 1.777b_t^4 + 3.259a_t^2b_t^2 - 1.022a_t^2 + 2.061b_t^2 \tag{61}$$

where we have neglected interference terms proportional to a_tb_t,$a_t^3b_t$ and $a_tb_t^3$ as their contribution was about a thousandth of the other terms in (61). The experimental results in [25] show that, at 139 fb^{-1}:

$$\mu_{t\bar{t}t\bar{t}}^{Exp} = 2^{+0.58}_{-0.50} \tag{62}$$

whereas for predictions regarding higher integrated luminosities:

$$\mu_{t\bar{t}t\bar{t}}^{300} = 1^{+0.39}_{-0.34} \quad \mu_{t\bar{t}t\bar{t}}^{3000} = 1^{+0.12}_{-0.11} \tag{63}$$

The allowed parameter space at the 1σ CL is then, using (62) and (63):

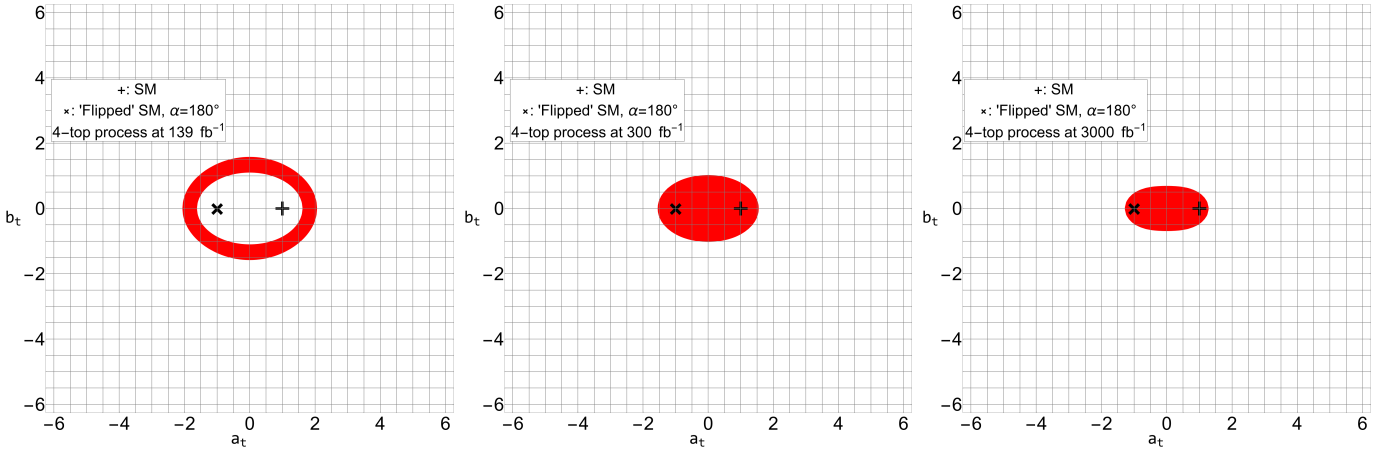

(a) (b) (c)

Figure 18: Parameter space consistent at the 1σ CL with (a) the measurement at 139 fb^{-1} of the 4-top process inclusive LO cross section, (b) the prediction at 300 fb^{-1} and (c) at 3000 fb^{-1} involving no new physics. The upright cross represents the SM and the slanted one is the 'Flipped' SM ($-y_t$).

In the last two processes considered, the top quark shows up in a virtual loop rather than in the final state: because of this the prediction for these processes are model dependent, in the sense that the results will depend on whether we include possible

new physics in the loops or not. Also note that bottom quarks loops will not be considered as they are generally negligible at an inclusive level. Despite not involving direct top-quark measures, these channels are generally measured (relatively) easily at the LHC, and therefore will be analyzed.

We firstly consider Higgs production through gluon-gluon fusion ggX_0 which is mediated by a triangular loop of heavy quarks, generally the top-quark being the largest contributor to the inclusive cross section and to a lesser extent the bottom quark; this channel for Higgs production was well described in the second chapter.
In this thesis we consider gluon fusion mediated by a top-quark loop for which, combining eq. (3.57) in [1] and eq. (3.8) in [26], the analytic inclusive cross section is (using the parametrization (50)):

$$\sigma(ggX_0) = \frac{G_\mu \alpha_s^2 M_X^2}{288\sqrt{2}\pi} \left| a_t \frac{3}{4} A_{\frac{1}{2}}^H(\tau_f) + i b_t \frac{3}{4} A_{\frac{1}{2}}^A(\tau_f) \right|^2 \tag{64}$$

where $\alpha_s \simeq 0.119$ is the strong coupling constant, M_X is the mass of the resonance, which we set now to 125 GeV and G_μ is given by (25). The form factors for spin-1/2 and spin-1 particles are given by:

$$A_{\frac{1}{2}}^H(\tau) = 2[\tau + (\tau - 1) f(\tau)]\tau^{-2} \tag{65a}$$

$$A_{\frac{1}{2}}^A = 2\tau^{-1} f(\tau) \tag{65b}$$

These form factors are defined so that for large top masses, $A_{\frac{1}{2}}^H$ reaches 4/3 and $A_{\frac{1}{2}}^A$ reaches 2; in this limit it is easy to see that the cross section is equivalent to the SM (in the same limit), which is the constant in front of the formula in (64). The function $f(\tau)$ is defined by:

$$f(\tau) = \begin{cases} \arcsin^2(\sqrt{\tau}) & \tau \leq 1 \\ -\frac{1}{4}[\log \frac{1+\sqrt{1-\tau^{-1}}}{1-\sqrt{1-\tau^{-1}}} - i\pi]^2 & \tau > 1 \end{cases} . \tag{66}$$

and the parameters $\tau_i = \frac{M_X^2}{4M_i^2}$ are defined by the masses $i = t, W$ of the particles involved in the loop.
Note also that since we just set M_X to 125 GeV, the only branch of the function $f(\tau)$ that is needed is $\tau \leq 1$ for both the top quark and the weak bosons.
Experimental results [27] show a ratio between the observed cross section for ggX_0 and the SM one at 139 fb^{-1} to be the following:

$$\mu_{ggX_0}^{Exp} = 0.96 \pm 0.10(\text{stat}) \pm 0.03(\text{exp}) \pm 0.03(\text{th}) \tag{67}$$

whereas predictions for higher integrated luminosities yield:

$$\mu_{ggX_0}^{300} = 1 \pm 0.074 \quad \mu_{ggX_0}^{3000} = 1 \pm 0.023 \tag{68}$$

Therefore the allowed parameter space at the 1σ CL is:

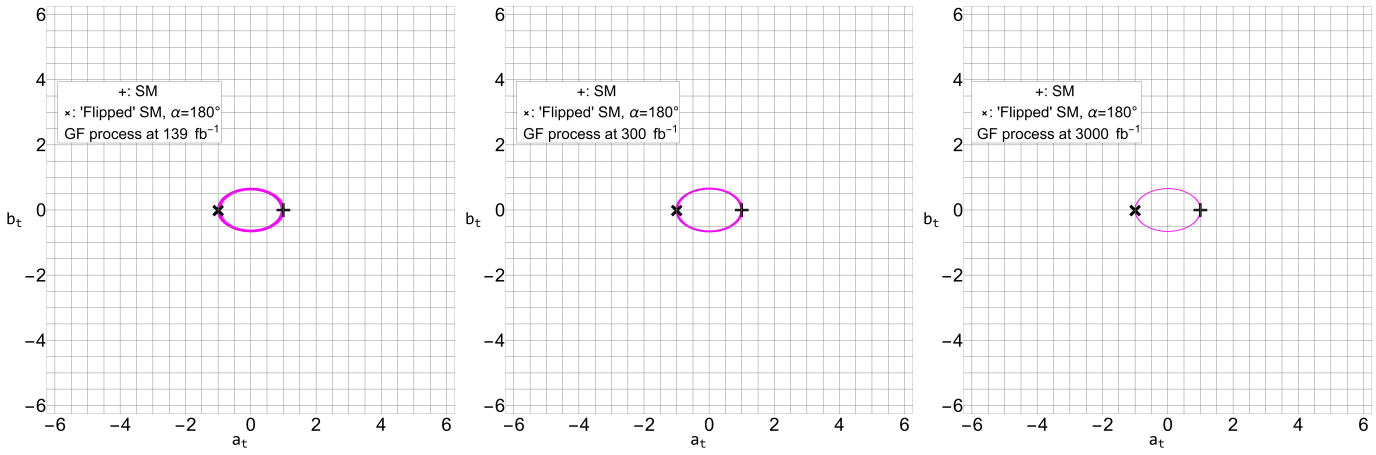

(a) (b) (c)

Figure 19: Parameter space consistent at the 1σ CL with (a) the measurement at 139 fb^{-1} of the gluon fusion cross section, (b) the prediction at 300 fb^{-1} and (c) at 3000 fb^{-1} involving no new physics. The cross represents the SM.

At last we consider the Higgs resonance decay into photons ($X_0 \to \gamma\gamma$), which occurs at the quantum level through a loop involving massive particles that couple to the Higgs, since the latter cannot interact with massless particles directly.
The decay into two photons is mediated primarily by loops of top-quarks and massive W bosons:

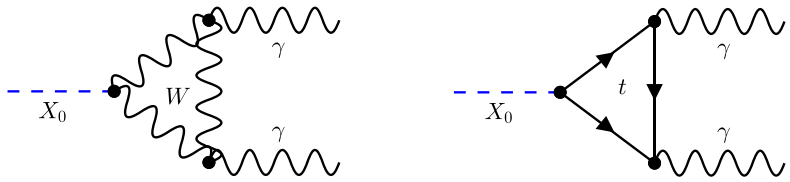

(a) (b)

Figure 20: Illustrative Feynman diagrams for the decay of the Higgs into two photons $X_0 \to \gamma\gamma$ mediated by a loop of (a) weak bosons and (b) quarks .

The partial decay width of Figure 20(a) and (b) can be obtained analytically both for the SM Higgs, eq. (2.45) in [1], and for a scalar resonance, eq. (2.24) in [26]. Parametrizing the interaction with the top-quark using (50) and leaving the one with the weak bosons in the SM, we get the total decay width:

$$\Gamma(X_0 \to \gamma\gamma) = \frac{G_\mu \alpha^2 M_X^3}{128\sqrt{2}\pi} \left| a_t N_c Q_t^2 A_{\frac{1}{2}}^H(\tau_t) + A_1^H(\tau_W) + i b_t N_c Q_t^2 A_{\frac{1}{2}}^A(\tau_t) \right|^2 \tag{69}$$

where

$$A_1^H(\tau) = -[2\tau^2 + 3\tau + 3(2\tau - 1)f(\tau)]\tau^{-2} \tag{70}$$

and now α is the fine structure constant given by (40), whereas Q_t is the charge of the top-quark and N_t its number of colors.
We note that in both GF and $H\gamma\gamma$ we assumed that no new physics takes place in the virtual top loop, like in Figure 2(a) and Figure 20, i.e. only SM virtual particles couple to the bosons and no net BSM cancelling effects occur; for this very reason both of those channels are heavily model dependent. At an integrated luminosity of 137 fb^{-1} recent reports [28] have shown that the ratio between the $X_0\gamma\gamma$ BR to the SM prediction, which we dub $\tilde{\mu}$, is:

$$\tilde{\mu}^{Exp}_{X_0\to\gamma\gamma} = 1.12 \pm 0.09 \tag{71}$$

whereas prediction for 300 fb^{-1} and 3000 fb^{-1} yield:

$$\tilde{\mu}^{300}_{X_0\to\gamma\gamma} = 1 \pm 0.061 \quad \tilde{\mu}^{3000}_{X_0\to\gamma\gamma} = 1 \pm 0.019 \tag{72}$$

Thus, at the 1σ CL the allowed parameter space for the three cases above is the following:

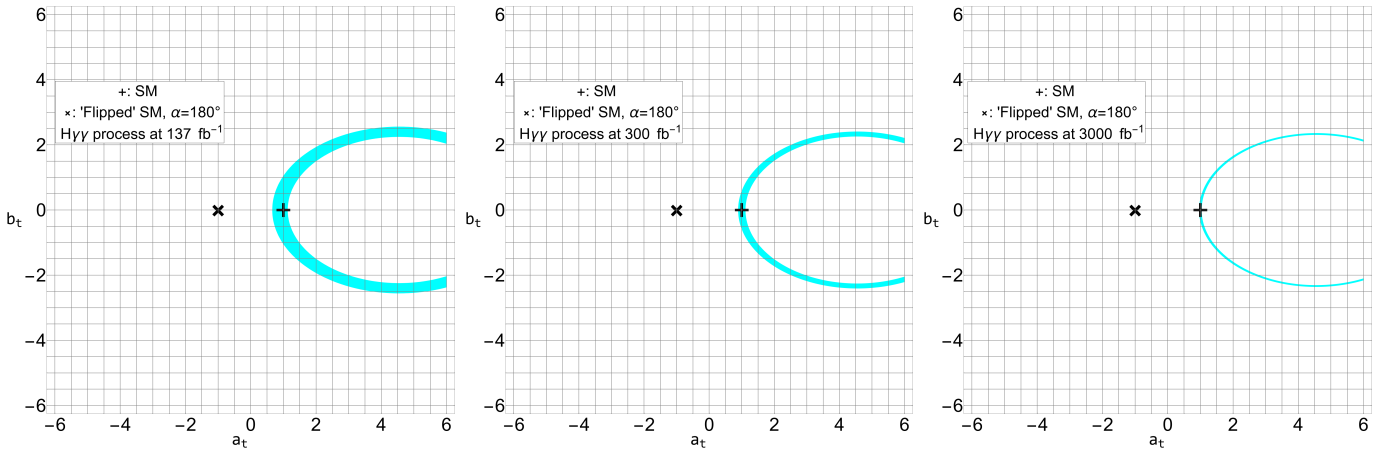

(a) (b) (c)

Figure 21: Parameter space consistent at the 1σ CL with (a) the measurement at 137 fb^{-1} of the Higgs decay into two photons BR, (b) the prediction at 300 fb^{-1} and (c) at 3000 fb^{-1} involving no new physics. The cross represents the SM.

Here, as in single top production, the diagrams in Figure 20 interfere, leading to linear terms (in a_t and b_t) in the total cross section which shift the ellipses in Figure 21.

Finally, these exclusion graphs put stringent bounds on the mixing angle α, at current LHC luminosities:

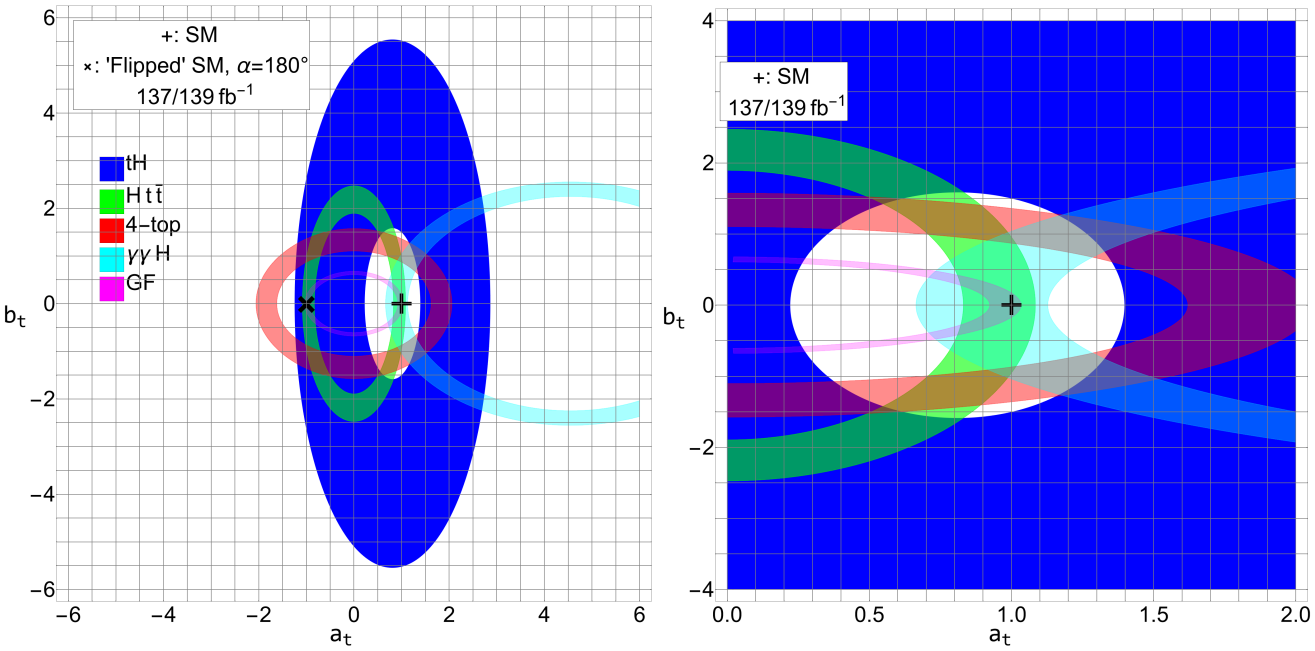

(a) (b)

Figure 22: Allowed parameter space at the 1σ CL for all processes that were analyzed, at the current LHC luminosities (139 fb^{-1} or 137 fb^{-1}). The upright cross is the SM and the slanted one is the 'Flipped' SM.

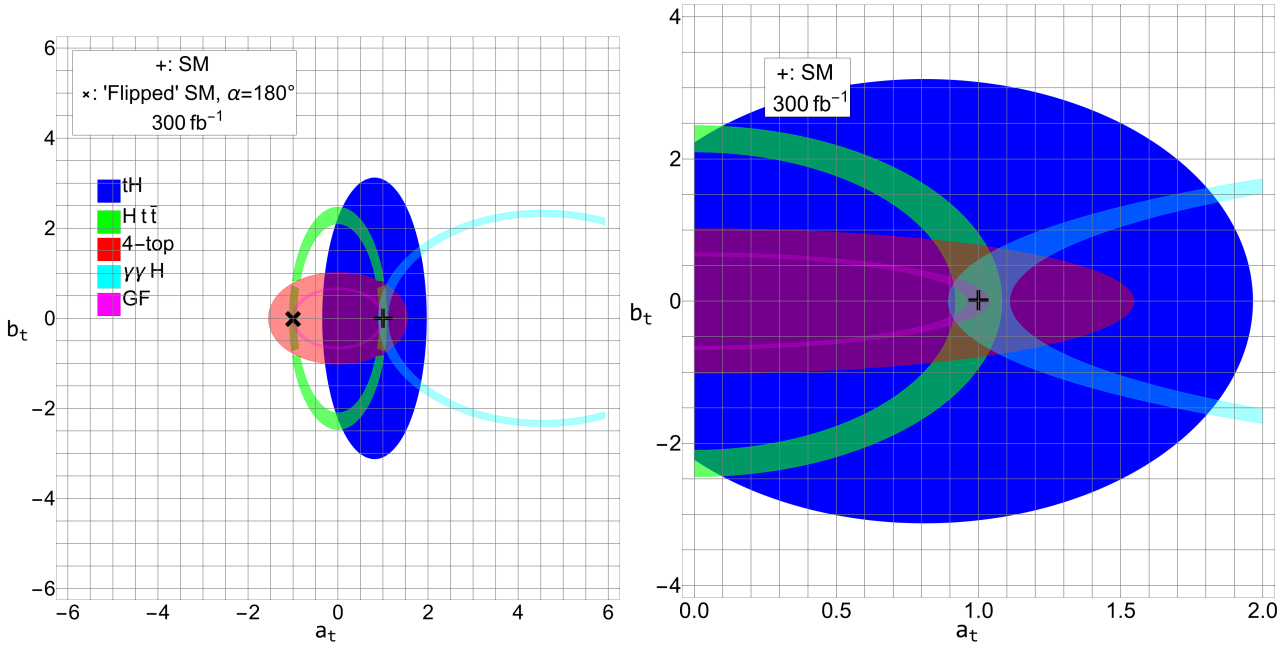

(a) (b)

Figure 23: Allowed parameter space at the 1σ CL for all processes that were analyzed, at higher luminosities and assuming the Standard Model (300 fb^{-1}). The upright cross is the SM and the slanted one is the 'Flipped' SM.

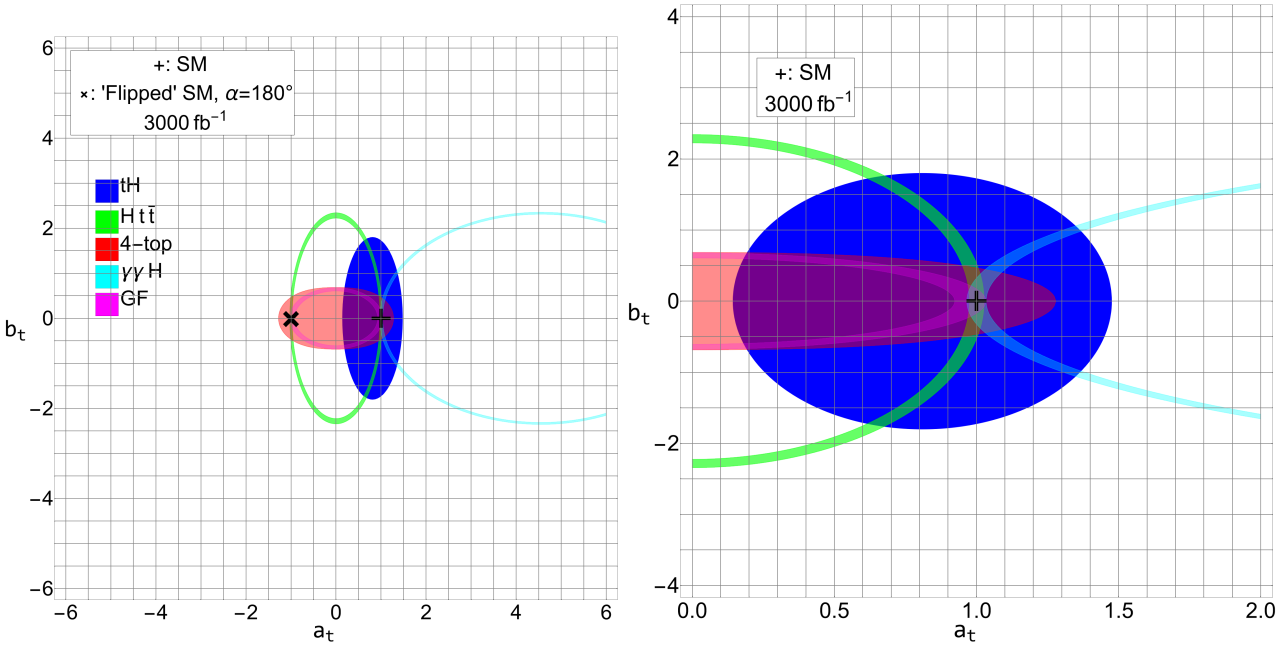

(a) (b)

Figure 24: Allowed parameter space at the 1σ CL for all processes that were analyzed, at higher luminosities and assuming the Standard Model (3000 fb^{-1}). The upright cross is the SM and the slanted one is the 'Flipped' SM.

We start by noting that in Figure 22 it's clear that both the tH and $t\bar{t}t\bar{t}$ channels are not compatible at the 1σ CL with the Standard Model top Yukawa coupling, however as was hinted at before, both of them suffer from imprecise results that are owed to the difficulty of the measurement of their inclusive cross sections at the LHC.
It is also of interest the fact that the GF and $t\bar{t}H$ channel, taking them alone, allow for both SM and Flipped Standard Model (FSM) interactions, this being a natural consequence of (52) and (64). However the $H\gamma\gamma$ channel is dependent also on the sign of the top-Higgs interaction (69), therefore once the measurement of the LHC returns a ratio (of measured to Standard Model Higgs branching ratios) close to one (71), the SM is the only scenario possible between it and the FSM.
In summary, excluding by virtue of imprecise measurements the tH and $t\bar{t}t\bar{t}$ channels, the other three processes put bounds of about 5% on a_t around the SM value, whereas non SM couplings (b_t) deviate from zero of about 20%.
Our predictions for 300 fb^{-1} and 3000 fb^{-1} take the Standard Model as a starting point and give possible future bounds on the parameters: a_t drops to 3% around 1 and b_t remains in an interval of approximately 20% centered around 0 for 300 fb^{-1}, whereas at 3000 fb^{-1} a_t is centered on 1 in a 2% interval and finally b_t drops to an interval of 15% around 0.

5 Conclusions and outlook

Starting from the Standard Model of particles and taking data from experiments which suggested that the weak bosons were in fact massive, we were forced to introduce a symmetry breaking mechanism that could explain these masses while retaining the overall gauge symmetry of the theory, this is also known as the "Higgs mechanism", which was also extended to generate fermion masses by Weinberg.
The mechanism predicted a particle, the Higgs boson, associated to the Higgs field, that would couple to the particles and endow them with their respective masses. In 2012 a particle of mass $\sim 125\ GeV$ was found at the LHC, and since then the physics community has been trying to verify if this is in fact the newly predicted SM particle.
A fundamental tool in calculating predictions for cross sections are the notorious "Feynman diagrams", which are of particular value as they offer a mechanical (nice for computers) way of doing calculations, and in fact programs for these type of estimates were built, like MadGraph5_aMC@NLO.
Aiding ourselves with these tools we parametrized the Higgs-top coupling (making no initial SM assumptions), and studying various processes (involving the said coupling): $t\bar{t}H$, tH,$t\bar{t}t\bar{t}H$, gluon fusion and $H \to \gamma\gamma$ decay, combined with the experimental results of ATLAS and CMS we put bounds on the parameters. The complementarity of all these channels is key for the results, in fact some processes taken by themselves are not dependent on the sign of the coupling constant, rendering difficult to pinpoint exactly the allowed values of the parameters, whereas other processes, being very challenging to measure at the LHC, necessarily yield very imprecise results; finally processes like GF and $H\gamma\gamma$ occur through a top-quark loop, and the assumption was made that no new physics takes place inside the loop, therefore making them heavily model dependent.
Results for current LHC luminosities bounded our parameters in the following way (at the 1σ CL): a_t appears to be centered around 1 (SM value) in a 5% interval and b_t is centered on 0 (SM) in a 20% interval.
Assuming no BSM physics takes place at future LHC luminosities (300 fb^{-1} and 3000 fb^{-1}), we made predictions on the "rigidity" of the bounds, assuming that uncertainties scale as the square root of the integrated luminosity. The results for these predictions show that at 300 fb^{-1} the interval of a_t shrinks to 3% and remains around the same for b_t, whereas at 3000 fb^{-1} the intervals drop to 2% and 15%.
This work presents certain limitations, such as the fact that we assumed no theoretical (i.e. on our models) and systematical uncertainties and that a realistic prediction for these processes would need to take into account at least NLO QCD corrections in the presence of an anomalous top-Higgs coupling (which in any case reduce the theoretical uncertainty).
While for most of the processes considered here such corrections are available, this is not the case for $t\bar{t}t\bar{t}$, for this process QCD and EW corrections mix together, and the latter require the SM relation between the top mass and Yukawa [29].
Finally, this thesis provides a study of the various processes at an inclusive level, while a more complete description would need to involve a further investigation at a differential level.

References

[1] A. Djouadi, "The Anatomy of electro-weak symmetry breaking. I: The Higgs boson in the standard model," *Phys. Rept.*, vol. 457, pp. 1–216, 2008.

[2] S. Weinberg, "A Model of Leptons," *Phys. Rev. Lett.*, vol. 19, pp. 1264–1266, 1967.

[3] C. Anastasiou, C. Duhr, F. Dulat, E. Furlan, T. Gehrmann, F. Herzog, A. Lazopoulos, and B. Mistlberger, "High precision determination of the gluon fusion Higgs boson cross-section at the LHC," *JHEP*, vol. 05, p. 058, 2016.

[4] P. Bolzoni, F. Maltoni, S.-O. Moch, and M. Zaro, "Higgs production via vector-boson fusion at NNLO in QCD," *Phys. Rev. Lett.*, vol. 105, p. 011801, 2010.

[5] D. de Florian *et al.*, "Handbook of LHC Higgs Cross Sections: 4. Deciphering the Nature of the Higgs Sector," vol. 2/2017, 10 2016.

[6] G. Aad *et al.*, "Observation of a new particle in the search for the Standard Model Higgs boson with the ATLAS detector at the LHC," *Phys. Lett. B*, vol. 716, pp. 1–29, 2012.

[7] S. Chatrchyan *et al.*, "Observation of a New Boson at a Mass of 125 GeV with the CMS Experiment at the LHC," *Phys. Lett. B*, vol. 716, pp. 30–61, 2012.

[8] A. M. Sirunyan *et al.*, "Evidence for Higgs boson decay to a pair of muons," *JHEP*, vol. 01, p. 148, 2021.

[9] A. M. Sirunyan *et al.*, "Observation of $t\bar{t}H$ production," *Phys. Rev. Lett.*, vol. 120, no. 23, p. 231801, 2018.

[10] M. Aaboud *et al.*, "Observation of Higgs boson production in association with a top quark pair at the LHC with the ATLAS detector," *Phys. Lett. B*, vol. 784, pp. 173–191, 2018.

[11] A. M. Sirunyan *et al.*, "Observation of Higgs boson decay to bottom quarks," *Phys. Rev. Lett.*, vol. 121, no. 12, p. 121801, 2018.

[12] M. Aaboud *et al.*, "Observation of $H \to b\bar{b}$ decays and VH production with the ATLAS detector," *Phys. Lett. B*, vol. 786, pp. 59–86, 2018.

[13] A. M. Sirunyan *et al.*, "Observation of the Higgs boson decay to a pair of τ leptons with the CMS detector," *Phys. Lett. B*, vol. 779, pp. 283–316, 2018.

[14] M. Aaboud *et al.*, "Cross-section measurements of the Higgs boson decaying into a pair of τ-leptons in proton-proton collisions at $\sqrt{s} = 13$ TeV with the ATLAS detector," *Phys. Rev. D*, vol. 99, p. 072001, 2019.

[15] R. D. Klauber, *Student Friendly Quantum Field Theory:: Basic Principles and Quantum Electrodynamics*. Fairfield, Iowa: Sandtrove Press, 2013.

[16] J. Alwall, M. Herquet, F. Maltoni, O. Mattelaer, and T. Stelzer, "MadGraph 5 : Going Beyond," *JHEP*, vol. 06, p. 128, 2011.

[17] F. Maltoni and T. Stelzer, "MadEvent: Automatic event generation with MadGraph," *JHEP*, vol. 02, p. 027, 2003.

[18] G. Aad *et al.*, "Evidence for the spin-0 nature of the Higgs boson using ATLAS data," *Phys. Lett. B*, vol. 726, pp. 120–144, 2013.

[19] P. Artoisenet *et al.*, "A framework for Higgs characterisation," *JHEP*, vol. 11, p. 043, 2013.

[20] F. Demartin, F. Maltoni, K. Mawatari, B. Page, and M. Zaro, "Higgs characterisation at NLO in QCD: CP properties of the top-quark Yukawa interaction," *Eur. Phys. J. C*, vol. 74, no. 9, p. 3065, 2014.

[21] A. M. Sirunyan *et al.*, "Measurement of the Higgs boson production rate in association with top quarks in final states with electrons, muons, and hadronically decaying tau leptons at $\sqrt{s} = 13$ TeV," *Eur. Phys. J. C*, vol. 81, no. 4, p. 378, 2021.

[22] F. Demartin, F. Maltoni, K. Mawatari, and M. Zaro, "Higgs production in association with a single top quark at the LHC," *Eur. Phys. J. C*, vol. 75, no. 6, p. 267, 2015.

[23] Q.-H. Cao, S.-L. Chen, and Y. Liu, "Probing Higgs Width and Top Quark Yukawa Coupling from $t\bar{t}H$ and $t\bar{t}t\bar{t}$ Productions," *Phys. Rev. D*, vol. 95, no. 5, p. 053004, 2017.

[24] Q.-H. Cao, S.-L. Chen, Y. Liu, R. Zhang, and Y. Zhang, "Limiting top quark-Higgs boson interaction and Higgs-boson width from multitop productions," *Phys. Rev. D*, vol. 99, no. 11, p. 113003, 2019.

[25] G. Aad *et al.*, "Measurement of the $t\bar{t}t\bar{t}$ production cross section in pp collisions at $\sqrt{s}$=13 TeV with the ATLAS detector," 6 2021.

[26] A. Djouadi, "The Anatomy of electro-weak symmetry breaking. II. The Higgs bosons in the minimal supersymmetric model," *Phys. Rept.*, vol. 459, pp. 1–241, 2008.

[27] G. Aad *et al.*, "Higgs boson production cross-section measurements and their EFT interpretation in the 4ℓ decay channel at $\sqrt{s}$ =13 TeV with the ATLAS detector," *Eur. Phys. J. C*, vol. 80, no. 10, p. 957, 2020. [Erratum: Eur.Phys.J.C 81, 29 (2021), Erratum: Eur.Phys.J.C 81, 398 (2021)].

[28] A. M. Sirunyan *et al.*, "Measurements of Higgs boson production cross sections and couplings in the diphoton decay channel at $\sqrt{\mathrm{s}} = 13$ TeV," *JHEP*, vol. 07, p. 027, 2021.

[29] R. Frederix, D. Pagani, and M. Zaro, "Large NLO corrections in $t\bar{t}W^{\pm}$ and $t\bar{t}t\bar{t}$ hadroproduction from supposedly subleading EW contributions," *JHEP*, vol. 02, p. 031, 2018.